Influence of body weight at young adulthood on the epigenetic clock and lifespan in the BXD murine family

Jose Vladimir Sandoval-Sierra[1], Alexandra H. B. Helbing[1], Evan G. Williams[3], David G. Ashbrook[2], Suheeta Roy[2], Robert W. Williams[2], Khyobeni Mozhui[1,2*]

[1]Department of Preventive Medicine, University of Tennessee Health Science Center, Memphis, Tennessee, USA

[2]Department of Genetics, Genomics and Informatics, University of Tennessee Health Science Center, Memphis, Tennessee, USA

[3] Department of Biology, Institute of Molecular Systems Biology, ETH Zurich, Zurich CH-8093, Switzerland

[*]Corresponding author: Kmozhui@uthsc.edu

Abstract

Background. The DNA methylation landscape is shaped by genetic and environmental factors and is modulate by aging. Here we evaluate the "aging methylome" in 12 recombinant inbred mouse strains from the BXD family that have more than two-fold variation in longevity. We examine relations among body weight, diet, lifespan, and DNA methylation-based rate of biological aging. We used affinity capture with the methyl-CpG binding domain (MBD) protein, followed by deep sequencing (MBD-seq), to assay DNA methylation in 70 mostly female liver samples, ranging in age from 6 to 25 months from mice maintained either on low fat chow or high fat diet (HFD).

Results. Genetic background among strains is a major source of variation in genome-wide DNA methylation patterns. Surprisingly, body weight at young adulthood had a stronger association with the methylome than age itself. Nonetheless, age also had a strong effect on methylation at well-defined CpG regions largely located within genes. We used subsets of age-informative CpGs to build versions of the epigenetic clock and as expected, these were strongly correlated with chronological age. Both high initial body weight and the HFD were associated with accelerated epigenetic aging. A DNA methylation clock model built using CpGs associated with body weight correlated with longevity of strains rather than chronological age, implying an underlying lifespan clock. Complementary mRNA clocks were also informative of chronological age. **Conclusion.** Our results support the known association between body mass and lifespan, and indicate that the methylome provides a mechanistic link to accelerated aging.

Keywords: Epigenetic clock, DNA methylation, aging, lifespan, longevity, age acceleration

Background

In the past few years, the "epigenetic clock" has emerged as a robust and widely used biomarker of aging that perhaps surpasses telomere length assays in its accuracy and utility [1-3]. Also referred to as the DNA methylation age (DNAmAge), the CpG based estimator of biological age comes in a few different versions for both humans and mice [4-11]. All these clocks share a common feature—they rely on the methylation status of preselected subsets of CpGs that are each assigned weights and are used collectively to estimate age. A critical question has been: are these DNAmAge clocks detecting changes that are purely a function of time and, therefore, correlates of chronological age? Or are they providing a measure of the intrinsic pace of biological aging that can be related to health, fitness, and life expectancy? Evidence from retrospective human epidemiological studies indicates that certain versions of the clock perform better at predicting life expectancy. In general, a younger DNAmAge relative to chronological age is associated with lower risk of disease and mortality [6, 12-18]. The age-dependent CpGs have also been studied in the context of lifespan variation among mammalian species [19], as well as variation within species, for example when lifespan is shifted by caloric restriction, treatment with rapamycin, or single gene mutations [7, 9, 10, 20-22].

As is the case with humans, aging trajectories vary considerably among mouse genotypes, and common DNA variants contribute to the pace of normal aging [23]. The BXD family has a long history in model organism aging and longevity research with median longevities of females ranging from at least 400 to 900 days [24-28]. Genomes of the BXDs are randomly recombinant versions of genomes of their two parents—strains C57BL/6J (B6) and DBA/2J (D2). On average,

56 D2 has a shorter lifespan than B6 [29, 30]. The more "accelerated aging" profile of D2 is
57 consistent with other age-associated parameters such as more rapid thymic involution [31] and
58 replicative senescence of hematopoietic progenitor cells [25], and increased tail tendon
59 breakage in D2 compared to B6 [32, 33]. Variation in lifespan is much greater among the
60 progeny BXD strains due to random assortment of independent gene variants [25].

61 Here, we have leveraged extensive experimental longevity data generated for the BXD family
62 [28] to evaluate the associations between body weight, DNA methylation, aging, and lifespan.
63 We used an affinity-capture enrichment followed by deep sequencing (MBD-seq) to profile the
64 liver methylome in 12 members of the BXD family [34-36]. To evaluate the impact of a
65 common metabolic stressor on aging, we also quantified the methylome of a subset of cases
66 maintained on a high fat diet (HFD), which is known to decrease the longevity by as much as
67 ~13% in the BXDs [28]. The main question we posed was: can we define DNA methylation clocks
68 that are predictive of strain and diet dependent variation in lifespan? And how do these relate
69 to strain characteristics such as body weight? Lastly, we tested whether age or lifespan
70 predicted by methylome patterns can be carried over to the transcriptome, and whether
71 transcripts can also be assembled into age-informative, and lifespan-predictive mRNA clocks.

72 Overall, the results reveal interdependence among body mass, the aging methylome, and
73 lifespan. In particular, body weight of young adults (ca. 100 days) has a pronounced effect of
74 DNA methylation. We were able to compute reasonably accurate DNAmAge estimates using
75 subsets of age-informative CpG regions. A similar clock using CpG regions associated with body
76 weight did not correlate with age, but was strongly correlated with strain lifespan. The clocks

77 highlight accelerated aging associated with higher initial body weight, and one version of the
78 DNAmAge estimator also showed accelerate aging on HFD. While mRNA-based clocks are a
79 feasible alternative, the methylome remains a more robust biomarker for aging and life
80 expectancy.

81 Results

82 Characteristics of the study sample

83 The longevity data was collected from a cohort of females that were allowed to age until
84 mortality. (Details on this cohort in Roy et al., 2019 [28] and full data can be accessed from
85 GeneNetwork 2 [37].) A parallel cohort was used for biospecimen collection at different ages.
86 For the 12 selected strains and F1 hybrids, lifespans on *ad libitum* standard chow (control diet
87 or CD) ranged from an average of 417 ± 155 days (mean ± SD) to 933 ± 86 days (**Table 1**). HFD
88 generally reduces longevity, but with marked differences among strains [28]. Matched samples
89 from cases on HFD were included for five strains and sub-strains (**Table 1**). Each strain-by-diet
90 group was classified as short-lived (mean lifespan < 600 days), medium-lived (between 600 and
91 750 days), and long-lived (>800 days). A strain classified as long-lived on CD may also be
92 classified as short-lived on HFD, e.g., BXD65 (**Table 1**).

93 We performed methylome-wide assays in 70 liver samples collected from the strain and diet
94 groups at different ages. Since age and lifespan are the main variables of interest, liver
95 specimens were chosen so that distribution of age across the three lifespan groups are closely
96 matched **(Fig. 1a**; individual level sample information in **Table S1)**. We note that aside from

97 three male cases for BXD102, B6D2F1, and B6D2F1 (**Table 1**), all specimens were from females.
98 While the samples were not chosen on the basis of body or organ weight, there was significant
99 variation in body weight when the mice were initially weighed before introduction to HFD (**Fig.**
100 **1b)**. The F1s had higher body weights compared to BXDs on CD, and this hybrid vigor was
101 apparent with or without the male cases. The final weight of mice (i.e., weight on day of sample
102 collection) continued to show significant strain variation (**Fig. 1b**). The weight of the liver
103 appeared fairly consistent across the strains (**Fig. 1b**). There was no group difference in body
104 weight at baseline between the two diets (CD = 25 ± 7 g vs. HFD = 23 ± 5 g; n = 70). By final
105 weighing, the group on HFD had become significantly heavier when compared to the full set of
106 mice on CD (HFD = 41 ± 12 vs. CD = 29 ± 8 g, $p < 0.0001$; n = 70), or when compared only to the
107 matched strains on CD (HFD = 41 ± 12 vs. CD = 26 ± 6 g, $p < 0.0001$; n = 34). The weight of the
108 liver on HFD was slightly heavier but the effect was not statistically significant, likely due to the
109 modest sampling of cases on HFD (HFD = 1.29 ± 0.23 g vs. CD = 1.22 ± 0.23 g; p = 0.37, n = 34).
110 The baseline weight was measured at young adulthood (mean age of 134 ± 81 days) and at this
111 point, age was a significant predictor of body weight with lower body weight for the younger
112 mice (**Fig. 1c**). The age of mice at time of sample collection was, however, not correlated with
113 final body weight (r = 0.01) or with weight of liver (r = 0.12). Instead, the baseline body weight
114 remained a significant predictor of the final body weight **(Fig. 1d)** and liver weight **(Fig. 1e)**.
115 When restricted to only the few HFD mice, baseline weight was still a significant correlate of
116 final body weight (r = 0.53, p = 0.05, n = 15), but not liver weight (r = 0.28, p = 0.30).

117

118 **Table 1. Characteristics of selected strains from the BXD panel**

	Longevity trait				Biospecimen	
Strain/line	Mean lifespan (days) [1]	Median lifespan (days) [1]	Lifespan Group [2]	Diet [3]	N [3]	Age Range (days) [3]
B6D2F1	933±86	896	long	CD	5 [4]	216–726
BXD102	861±222	891	long	CD	5 [4]	183–714
BXD40	585±239	577	short	CD	8	284–719
BXD48	695±124	684	med	CD	3	188–731
BXD48	523±152	517	short	HFD	3	189–595
BXD48a	617±196	670	med	CD	3	233–604
BXD48a	635±113	650	med	HFD	3	233–543
BXD65	824±199	896	long	CD	6	181–711
BXD65	534±128	551	short	HFD	3 [5]	230–541
BXD65b	726±91	751	med	CD	4	187–748
BXD73	702±116	687	med	CD	4	206–759
BXD73	699±112	715	med	HFD	3	206–694
BXD73b	820±129	807	long	CD	3	237–743
BXD73b	742±193	790	med	HFD	3	237–729
BXD79	417±155	330	short	CD	7	217–570
BXD9	507±135	462	short	CD	3	245–548
D2B6F1	771±143	791	long	CD	4 [4]	210–744

119 [1] Average and median lifespans for strains under standard or high fat diet estimated from an aging cohort of mice
120 co-housed with mice used for biospecimen collection and methylome assays
121 [2] Groups based on phenotypic lifespan: short = average lifespan < 600 days; med = average 640–750 days, and long
122 = average lifespan > 800 days
123 [3] Diet, sample size, and age range of mice from MBD-seq data was generated. CD = control diet; HFD = high fat diet
124 [4] One male case; see Table S1 for individual level data
125 [5] One case excluded due to uncertain identity
126

127 Strain dependent patterns in global features of the methylome

128 Deep sequencing of the methylome was carried out after samples were enriched for
129 methylated-CpGs (MBD-seq). After quality checks and filtering by read coverage, we retained a
130 set of 368,300 regions, each 150 bp in length, with sufficient coverage in the 70 samples. The
131 majority of the CpG regions (83%) contained no sequence variants (SNPs or small
132 insertions/deletions) segregating in the BXDs. For the 17% with sequence variants, there was

133 an average of 2 ± 1.6 variants within the 150 bp bin. (Chromosomal coordinates, CpG density,
134 variant counts, and normalized data will be made available from NCBI GEO upon official
135 publication.) Consistent with the DNA enrichment and filtering protocols, the 368,300 CpG
136 regions were enriched in annotated gene features and CpG islands and depleted in intergenic
137 regions when compared to the genome-wide background (**Table S2**). Our first goal was to gain a
138 global perspective, and for this, we performed two analyses: (1) dimension reduction with
139 principal component analysis (PCA), and (2) analysis of genome-wide mean methylation and
140 variance.

141 PC1 and PC2 captured 19% and 13% of the variance, respectively. A plot of the top two
142 principal components (PCs) showed clustering of samples by strain identity, irrespective of diet
143 (**Fig. 2a**). The one exception was a BXD65 on HFD; this case plotted away from the BXD65
144 cluster and, as this was of questionable identity, this sample was excluded from downstream
145 analyses. Sub-strains (e.g., BXD73/BXD73b; BXD65/BXD65b) also clustered in close proximity
146 with only slight separation. Unsupervised hierarchical clustering confirmed the clustering of
147 samples by strain identity rather than age or diet groups (QC plots in **Fig. S1**). The top five PCs
148 collectively explained 58% of the variance (PC1–PC5 in **Table S1**). We found no correlation
149 between these five PCs and the age of mice. For strains with matched CD and HFD cases, the
150 PCs did not differentiate between the two diets.

151 Next, we computed the within-individual genome-wide average methylation and variance.
152 Global average methylation was inversely correlated with within-individual variance and
153 showed extensive strain variability. When we divided the CpG regions into genic (i.e., CpG

154 regions that overlap annotated gene features) and intergenic sets, we found that the inverse
155 correlation between global methylation and variance was significant for both sets but
156 particularly pronounced for the intergenic set (**Fig. 2b, c;** and **Table S1** for individual level data
157 on methylome means and variance). This reveals that for CpGs in intergenic regions, mice that
158 have a hypermethylated profile have lower within-individual variance. There is extensive strain
159 variation in this global methylation and variance patterns (**Fig. 2b, c**). For the intergenic set, the
160 BXD73 sub-strains showed the lowest methylation scores and highest variance while the F1s
161 had the highest methylation and lowest variance. Age was not a significant correlate of the
162 genic and intergenic features. We evaluated if the top 5 PCs relate to the methylation averages
163 and variance. The average methylation and variance at intergenic CpG regions were
164 significantly correlated with PC1 (**Fig. 2d**), and PC3 (11% of variance) (**Fig. 2e**). PC4 (8% of
165 variance) showed a significant negative correlation with mean methylation at genic CpG regions
166 (**Fig. 2f**).

167 To summarize, the global analyses show that the clustering by strains in the PC plot, to a large
168 extent, can be explained by the strain-dependent methylation averages. We did not detect any
169 effect of age or diet on these large-scale methylome features.

170 Intercorrelations between body weight, methylome, and strain-level lifespan

171 We next examined whether the body weight measures could be associated with the large-scale
172 methylome features. Since the F1s exhibit hybrid vigor both in body weight and mean
173 methylation, we report the results after excluding the F1s (correlations with and without the
174 F1s in **Table S3**). Of the top 5 PCs, only PC1 showed a weak but significant negative correlation

175 with baseline weight (**Fig 3a**), and final weights of body and liver. Body weight at baseline, but
176 not the final body weight, had a weak but significant negative correlation with mean
177 methylation (**Fig 3b**), and significant positive correlation with variance (**Fig 3c**) at genic CpG
178 regions that indicates a sustained inter-relatedness between body mass at younger age and the
179 methylome. Unlike the baseline body weight, the final body weight was not correlated with
180 methylation means or variance at either the genic or intergenic regions in the BXDs (**Table S3)**.
181 We considered the possibility that the HFD-induced shifts in body weight may have reduced the
182 correlation; however, when we restricted the analysis to only the CD BXDs (n = 46), the final
183 body weight still showed no correlation with the intergenic and genic features. The liver weight
184 had a significant positive correlation with mean methylation and negative correlation with
185 variance at intergenic CpGs **(Table S3)**.

186 The lifespan data is from 17 strain-diet groups (**Table 1**), and while this is a small sampling of
187 lifespan variability in the BXD panel, we used this longevity information to explore associations
188 with the body weight measures and the global methylome features. This analysis was again
189 performed without the F1s due to the vigor in both methylome features, body weight, and
190 lifespan. Only PC4, an inverse correlate of genic CpG methylation means (**Fig. 2f**), showed a
191 strong correlation with the strain longevity phenotype (**Fig 3d**). Lifespan showed no direct
192 correlations with the methylation averages and variance at either the genic or intergenic CpG
193 regions. For the weight measures, baseline body weight had a weak but significant negative
194 correlation with strain mean lifespan (r = -0.27, p = 0.04; **Fig 3d**). This is in agreement with the
195 stronger inverse correlation between body weight and lifespan that is seen in the larger BXD
196 cohort [28].

197 Taken together, while the individual correlations are weak (**Fig 3**), the results suggest that body
198 weight at younger age is associated with multiple interdependent features of the global
199 methylome that are also predictive of strain life expectancy.

200 Effect of age on site specific DNA methylation

201 Following the global analyses, we next evaluated the effect of age and diet on site-specific DNA
202 methylation at each of the 368,300 CpG bins. Our goal was to identify age informative CpG
203 regions that we can then use to estimate the epigenetic age of mice. We applied a multiple
204 regression model for age and diet with adjustment for other major sources of variance
205 (methylation ~ age + diet + PC1 + PC2 + PC3 + PC4 + PC5). Although we did not detect a
206 generalized impact of aging on the global methylation, the distribution of *p*-values indicated a
207 strong effect on few CpG regions (**Fig. 4a**). For the effect of diet, the *p*-value distribution was
208 close to the null hypothesis (**Fig. 4b**), likely because with only 14 samples from the HFD group,
209 the sampling is underpowered. For the remainder, we focused mainly on age, and considered
210 diet only in the context of its effect on strain lifespan and potential age-accelerating effect.

211 At a Bonferroni threshold of 10% (unadjusted $p \leq 2.6 \times 10^{-7}$), there were 26 age-associated
212 differentially methylation regions (age-DMRs). All of these were genic regions, including
213 neighboring block of CpGs, and were located within 17 annotated genes **(Table S4)**. While only
214 a small number of CpG bins were significant at the 10% Bonferroni threshold, given the non-
215 independence of adjacent CpG regions, we used a lenient statistical threshold and selected the
216 top 500 age-DMRs to define the general characteristics of the aging methylome (unadjusted $p \leq$
217 3.1×10^{-4}, 23% FDR; Manhattan plot **Fig. 4c**; **Table S4**). Of these, 60% (299 of 500) were

218 associated with loss of methylation with age (age-hypomethylation), and 40% showed gains in
219 methylation with age (age-hypermethylation) [38, 39]. This set of 500 age-DMRs collectively
220 represented differentially methylated CpG regions located in or near 347 unique genes
221 (location within genes or distance to nearest promoter for intergenic CpG regions in **Table S4**).
222 Gene set enrichment analysis (GSEA) for the age-DMRs ranked by regression coefficient for age
223 showed no strong enrichment after FDR correction. However, we note that the most
224 overrepresented pathway was for signaling genes involved in stem cells pluripotency (KEGG ID
225 mmu04550; nominal enrichment p = 0.005, FDR = 0.10) and the five genes in this pathway
226 (*Fzd1*, *Fzd8*, *Wnt5a*, *Jak3*, *Meis1*) were associated with increase in DNA methylation with age.
227 Genes involved in mesenchyme development were also slightly overrepresented (GO ID
228 0060485; nominal enrichment p = 0.001, FDR = 0.24) and members of this GO (*Ptk7*, *Nrp2*,
229 *Sema5b*, *Zfp703*, and *Wnt5a*) were also associated with age-hypermethylation (**Fig. S2**).

230 Compared to the background set of 368,300 CpG bins, the age-DMRs were depleted in
231 intergenic regions and enriched in genic regions (enrichment and depletion p-values in **Table**
232 **S2**). The majority of the age-DMRs (86%) contained no sequence variants in the BXDs and the
233 age dependent methylation patterns are unlikely to be confounded by SNP or variant effects.
234 The age-hypermethylated set was highly enriched in CpG islands, promoters, and exons, and
235 also slightly enriched in 5'UTRs (**Fig. 4d**; **Table S2**). The age-hypomethylated set was enriched in
236 introns, and 3'UTRs and transcription termination sites (**Fig. 4d**; **Table S2**). For each CpG region,
237 we computed the average methylation and variance across the 69 samples, and compared
238 these to the age regression coefficients, which convey the change in methylation per unit
239 change in age. The most pronounced age-hypermethylation (positive regression coefficients for

240 age) occurred in bins with high CpG density and lower average methylation, and the magnitude
241 of the age coefficient showed positive correlation with CpG density and negative correlation
242 with average methylation (**Fig. 4e, f**). In contrast, age-hypomethylated regions (negative
243 regression coefficient for age) featured low CpG density, and higher average methylation (**Fig.**
244 **4e, f**).

245 Age-DMR based epigenetic clocks and lifespan prediction

246 We next explored constructing age-informative and potentially lifespan-predictive clocks using
247 three different approaches: (1) training-based age estimator by applying elastic net regression,
248 (2) untrained age estimator with the set of 500 age-DMRs, and (3) untrained age estimator
249 using only a subset of the age-DMRs that are also associated with cross-sectional variation in
250 lifespan.

251 First, we implemented the standard clock-building protocol by deriving the clock in a training
252 cohort, and then testing accuracy in a validation cohort [40, 41]. We are clearly limited in
253 sample size; nevertheless, as assessment of feasibility, we randomly assigned 36 samples (52%
254 of the 69 cases) to the training set to model an age-estimator (see **Table S1** for sample
255 assignments). This constructed an age-estimator that was based on 60 "clock CpGs", i.e., CpG
256 regions that are collectively used in determining the DNAmAge [5]. These clock CpGs included a
257 few regions that individually showed no significant association with age; but most had modest
258 to strong associations with age and included fifteen of the 500 age-DMRs (clock CpG regions
259 and weighing coefficients in **Table S5**). In the training set, this age estimates had a near perfect
260 correlation with chronological age at Pearson r = 0.999 (**Fig. 5a**; **Table 2**). In the test set of n =

261 33, the correlation between the estimated age and chronological age was 0.74 ($p < 0.0001$) with
262 a median absolute error of 90 days (**Fig. 5b**; **Table 2**). Due to the small sample size of the test
263 set, we did not use this clock to examine age acceleration.

264 For the non-training based estimator, we simply treated the 500 age-DMRs as possible clock
265 CpGs and used the respective age regression coefficients as weighing factors to compute the
266 weighted average for each sample (coefficients for each CpG region are in **Table S4**). The
267 weighted averages were significantly correlated with chronological age of mice, and for a more
268 direct comparison, the values were scaled to the age range for the 69 samples. This clock is
269 therefore study-specific and calibrated to this cohort. The DNAmAge had a near linear
270 correlation with chronological age at $r = 0.90$ ($p < 0.0001$), and with a median absolute error of
271 96 days (**Fig. 6a; Table 2**). We then estimated the age acceleration for each mouse (DNAmAge-
272 acc) based on the residuals derived from the linear regression between DNAmAge and
273 chronological age [9, 12] (individual-level DNAmAge data in **Table S1**). For this, positive residual
274 values indicate an accelerated, and negative values a decelerated rate of biological aging.
275 Unlike the DNAmAge, DNAmAge-acc was not correlated with the final age of mice, indicating
276 that this measure of age acceleration is independent of chronological age [9]. The DNAmAge-
277 acc derived from this clock did not correlate with the lifespan phenotype but showed a
278 significant positive correlation with body weight measures that would suggest a more
279 accelerated clock with increased body mass (**Fig. 6b, c**; **Table S6**). For the strains with matched
280 samples, the DNAmAge-acc did not differentiate between the diet groups (**Fig. 6d**).

281 We then examined if we can build a version of the DNAmAge estimator using only the age-
282 DMRs that were also associated with strain differences in expected lifespan. We limited this
283 analysis to the top 500 age-DMRs, and to test association with lifespan, we applied a mixed
284 effects model with strain median lifespan and age as fixed variables and strain-diet as random
285 variable. At a lenient statistical threshold of $p \leq 0.05$, there were 56 age-DMRs associated with
286 lifespan and we refer to this set as putative lifespan-age-DMRs (**Table S4**). The majority of these
287 (84% or 47 of 56) had lower methylation among the long-lived strains regardless of whether
288 these were age-hypermethylated or age-hypomethylated (**Fig. 7a**). We illustrate this pattern
289 using three of the top-ranking lifespan-age-DMRs: age-hypomethylated *Casz1* (**Fig. 7b**), and
290 age-hypermethylated *Cyp46a1* (**Fig. 7c**) and *Abca7* (**Fig. 7d**). *Casz1* was associated with a small
291 age-hypomethylation (age coefficient of only -0.0007, unadjusted $p = 1.6 \times 10^{-4}$) and most
292 strain-diet groups had slight downward trajectory over time. *Cyp46a1* and *Abca7*, on the other
293 hand, were associated with stronger age-hypermethylation, and almost all the strain-diet
294 groups showed an upward trajectory with age. In addition to the change over time, cross-
295 sectional comparison between lifespan groups showed lower average methylation in the long-
296 lived strains relative to the medium and short-lived strain-diet groups.

297 While most of the CpG regions were only weakly associated with lifespan (for instance, *Abca7* in
298 **Fig 7d**), we used the 56 lifespan-age-DMRs to calculate the DNAmAge by weighing each CpG by
299 the respectively age regression coefficients (estimated ages in **Table S1**). Chronological age
300 correlated strongly to this version of the DNAmAge ($r = 0.83$, $p < 0.0001$), although the trend
301 appeared to fit a quadratic equation with a greater degree of plateau at older age, an
302 observation that is consistent with the apparent underestimation or possible decline in aging

303 rate with increased chronological age [15, 42, 43] (**Fig. 6e**). The DNAmAge-acc derived from
304 this version of the clock showed a significant negative correlation with the longevity phenotype
305 (both mean and median lifespan) with more accelerated aging in mice from the short-lived
306 strain-diet groups (**Fig. 6f**). This correlation was robust and remained significant after excluding
307 the F1s (full correlation and probabilities in **Table S6**). The DNAmAge-acc was also positively
308 correlated with the body weight measures, again indicating more accelerated aging in mice
309 with higher body mass (**Fig. 6g, Table S6**). For the strains with matched samples from CD and
310 HFD, the group on HFD had a mean age acceleration of 21 ± 36 days compared to the mean
311 decelerated aging (-26 ± 57 days) for the group on CD (p = 0.01; n = 33; **Fig. 6h**). Therefore, this
312 DNAmAge estimator, built from fewer CpG regions, is therefore both age-informative and
313 lifespan-predictive.

314 **Table 2. Versions of DNA methylation and mRNA clocks**

Clock versions	Sample N	Clock CpGs/mRNAs	Age r[1]	median |error|[2] (days)	BW0 r[3]	Lifespan r[3]
DNA methylation elastic net	36 training	60	0.99 (<0.0001)	4.5	not tested	not tested
	33 testing		0.74 (<0.0001)	90	not tested	not tested
500 age-DMRs	69	500	0.9 (<0.0001)	96	0.38 (0.001)	0.004 (ns)
56 lifespan-ageDMRs	69	56	0.83 (<0.0001)	111	0.24 (0.05)	r = -0.58 (<0.0001)
500 BW0-DMRs	69	500	0.12 (ns)	*66	*r = -0.52 (<0.0001)	*0.47 (<0.0001)
RNA clock elastic net Ver1	150 training	65	0.89 (<0.0001)	52	not tested	not tested
	141 testing		0.65 (<0.0001)	85	-0.17 (0.05)	-0.15 (ns)
RNA clock elastic net	141 training	62	0.90 (<0.0001)	67	not tested	not tested

Ver2	150 testing	0.62 (<0.0001)	100	0.19 (0.02)	0.08 (ns)

[1] Pearson correlation between clock estimates and chronological age; significance within parenthesis
[2] Median of the absolute difference between estimated and chronological age as a measure of DNAmAge precision as defined in [40]. *For the 500 BW0-DMR clock, median of the absolute difference between estimates and mean lifespan was used as a measure of lifespan clock accuracy.
[3] Pearson correlation between age acceleration residuals and baseline body weight and strain mean lifespan. *For the 500 BW0-DMR clock, the estimated values instead of the residuals were used.

Baseline body weight based epigenetic clock and lifespan prediction

Given the strong influence on baseline body weight on the methylome, we then explored the possibility of deriving lifespan informative estimator from body weight associated CpG regions. To identify relevant CpG regions, we applied a regression analysis with baseline body weight (BW0) as predictor with adjustment for age and top 5 PCs as covariates. While age was associated with only a few strong age-DMRs, BW0 had a more widespread association with the methylome (**Fig. 8a**). At a Bonferroni threshold of 10% (unadjusted $p \leq 2.6 \times 10^{-7}$), there were 667 CpG regions associated with body weight. Unlike the age-DMRs, which were depleted in intergenic regions, 74% of the baseline body weight associated differentially methylated CpG regions (BW0-DMRs) were intergenic. The vast majority (581 of the 667) had positive regression estimates for body weight, i.e., higher levels of methylation in heavier mice.

As in the case of the age-DMR based clock, we then took the top 500 BW0-DMRs and weighed each CpG region by the respective age regression coefficient (weighing coefficients and the list of CpG regions in **Table S7**). We note that 27.6% (138 of the 500) of the BW0-DMRs contained sequence variants, and the differential methylation at these sites could also be capturing the effect of underlying sequence effects. Using the BW0-DMRs, the weighted averages did not

338 correlate with the chronological age of mice. Instead, the values had a significant positive
339 correlation with strain lifespan. For direct comparison, we rescaled the weighted averages to
340 the range of median lifespan for the study sample **(Fig. 8b**; **Table S1)**. The strong positive
341 correlation with lifespan suggests that this clock is an indicator of the expected age at death
342 rather than the chronological age of mice. The median absolute error for the predicted lifespan
343 relative to the known lifespan for the strain-diet groups was at 66 days (**Table 2**), and we refer
344 to this as a baseline body weight based lifespan clock (BW0.lifespan). For a few of the long-lived
345 strains, particularly the robust F1 hybrids that have both higher body weight and longer lifespan
346 (labelled as groups A and B **in Fig. 8b**), the BW0.lifespan was much lower than the expected
347 lifespan. Since the CpGs regions were individually associated with body weight, as expected, the
348 BW0.lifespan showed a strong correlation with the baseline weight (**Fig. 8c**) and with liver
349 weight, but not strongly with final body weight (**Table S6**). For strains that had both CD and HFD
350 cases, BW0.lifespan did not differentiate between the diet groups, suggesting that this clock is
351 not sensitive to lifespan modification by HFD but is mainly dependent on strain differences in
352 baseline body weight. The age acceleration residuals from the 56 lifespan-age-DMRs had a
353 strong inverse correlation with the BW0.lifespan estimates indicating convergent information
354 from both the clocks (**Fig. 8d**).

355 Impact on gene expression and mRNA based clocks

356 To examine age-dependent changes in the liver transcriptome, we made use of available liver
357 RNA sequencing (RNA-seq) data from a larger cohort of aging BXDs. The data obtained from
358 GeneNetwork was generated in two batches, and sample and batch information are in **Table**

359 **S8**. First, to examine whether the transcripts that correspond to the age-DMRs also show
360 changes in expression levels with age, the 347 unique genes represented by the 500 age-DMR
361 CpGs were matched to the corresponding transcripts by gene symbol. This resulted in 265 age-
362 DMRs and transcript pairs. Of these, 110 of the transcripts (42%) were correlated with age at an
363 unadjusted $p \leq 0.05$ ($|r| \geq 0.12$ in $n = 291$) (**Table S9**). The majority of the age-hypermethylated
364 CpG regions were associated with increased gene expression with age with only nine age-
365 hypermethylated DMRs (e.g., *Fzd8*, *Cyp46a1*, *Nfix*, *Rnf4*) associated with decreased gene
366 expression with age (**Table S9**). For the age-hypomethylated DMRs, 37 transcripts showed a
367 decrease in expression and 39 transcripts showed an increase in expression with age. Overall,
368 this shows that many of the age-DMRs are also associated with gene expression changes with
369 age.

370 Finally, we attempted to derive age-informative clocks using the training-based approach. We
371 first performed the training in batch 1 and then tested in batch 2, and then vice versa using the
372 liver transcriptome-wide data. The elastic net modeling trained on the 150 samples in batch 1
373 identified 65 transcripts for mRNA clock estimation (**Table S10**), and the age estimated from
374 these transcripts (mRNAage) had a correlation of $r = 0.89$ with chronological age in the training
375 set (**Fig. 5c**; **Table 2**). In the validation set (i.e., batch 2 with 141 samples), the correlation
376 between the age estimates and chronological age was 0.65 with median error of 85 days (**Fig.
377 5d**; **Table 2**). The age acceleration, as estimated by the residuals from the regression between
378 mRNAage and chronological age, showed a weak but significant ($p = 0.05$) negative correlation
379 with baseline body weight, which is at odds with the expected age acceleration with higher
380 body mass, and no significant correlation with strain lifespan (mRNA age estimates and age

381 acceleration for individual samples in **Table S8**). Training in batch 2 identified 62 transcripts for
382 clock estimation **(Table S11**). Of these 62 transcripts, only 9 transcripts (*Rin3*, *Adcy3*, *Cpn1*,
383 *Chuk*, *Rpl41*, *Rps27a*, *Serpina3m*, *Srm*, and *Ubb*) overlapped between the two versions of the
384 mRNA clocks. Correlation between the mRNAage and chronological age was 0.90 in the training
385 set, and 0.62 in the testing set (**Fig 5e**, **5f**; **Table 2**). The age acceleration for this version of the
386 clock showed a significant positive correlation with baseline body weight and no correlation
387 with lifespan (**Table S8**). For strains with samples from both CD and HFD, the age accelerations
388 derived from the mRNA clocks did not differentiate between diets.

389 Discussion

390 The results we have presented convey deep associations between body mass, DNA
391 methylation, aging, and lifespan. Somewhat to our surprise, we found that body weight at
392 young adulthood, more so than age at time of tissue collection, had a stronger influence on the
393 large-scale methylome. Age, on the other hand, had a strong effect on few discrete CpG
394 regions. Age and weight appeared to exert effects on largely independent sets of CpGs, with the
395 age-DMRs mostly located within gene bodies, while the BW0-DMRs included a large proportion
396 of intergenic loci. Nonetheless, longevity information could be derived from both the age- and
397 BW0-DMRs.

398 Consistency in age-dependent DNA methylation changes

399 In regard to whether genomic characteristics can explain whether a CpG region gains or loses
400 methylation with time, we found a clear dependence on CpG density and methylation status

401 that agreed with previous reports [44, 45]. Since DNA methylation levels were quantified over
402 150 bp non-overlapping bins, we could directly examine how the local CpG density relates to (1)
403 average methylation levels and variance across the 69 samples, and (2) the change over time
404 using the age regression coefficients. The results show that loss of methylation over time occurs
405 at regions with low CpG density that also generally have higher average methylation. This is
406 consistent with the general age-dependent hypomethylation at CpG spares regions of the
407 genome where the few or isolated CpGs exist mostly in a methylated state [46-49]. For age-
408 hypermethylated regions, the gains in methylation was directly correlated with CpG density,
409 and inversely correlated with methylation, and occurred in regions with lower average
410 methylation. This too, is consistent with reports that CpG dense regions on the genome, a
411 feature of CpG islands, which typically remain unmethylated, are the sites that tend to gain
412 methylation with age [50-53].

413 For the 347 unique genes that correspond to the 500 age-DMRs, we did not find a particularly
414 strong functional theme. However, the list included notable members that have previously
415 been linked to aging related diseases or with longevity and lifespan. For example, *Cyp46a1*, *Lrp1*
416 and *Abca7* play roles in lipid shuttle and cholesterol metabolism, and have been associated with
417 Alzheimer's disease [54, 55]. Other age-DMR genes that have been previously implicated in
418 aging and human longevity include *Adarb2* [56], *Abcc4* [57], *Igf2r* [58], *Ucp3* [59], *Grb2* [60], *Il7r*
419 [61], *Ikbkb* [62]. The current data replicated the CpG islands in *C1ql3* and *Ptk7*, which we
420 previously reported as age-hypermethylated sites in the BXD parental strains, C57BL/6J and
421 DBA/2J [63]. We also compared the list of age-DMRs from the present study to a list of 79
422 genes reported to harbor age-DMRs in a recent study of DNA methylation in aging human liver

423 [42], and found only three genes in common: *Il4i1*, *Ildr2* and *Nfix*. The study by Bacalini et al.
424 [42] reported an enrichment in mesenchymal and Wnt-signaling pathways, and similarly, we
425 also find a slight over-representation of genes that are part of signaling pathways and
426 mesenchyme development (e.g., *Fzd1*, *Fzd8*, *Wnt5a*, *Jak3*, *Ptk7*, *Nrp2*, etc.).

427 Building clocks from age dependent CpG regions

428 Currently, there are several different versions of the DNAmAge estimator available for both
429 mice and humans. Some have multi-tissue application [5, 8, 9], and others are optimized for
430 specific tissues [4, 7, 10, 11]. The standard protocol for developing DNAmAge clocks starts by
431 applying a linear regression algorithm in a training dataset, followed by age estimation in
432 validation cohorts to gauge the accuracy of the clock [5, 40, 41]. The training sessions identify
433 age informative CpGs, referred to as clock CpGs, that are each assigned predetermined weight
434 for estimating DNAmAge. This preselected ensemble of clock CpGs can then be used to
435 estimate age in other independent data sets, under the condition that the same or at least the
436 majority of the CpGs are also measured. To our knowledge, all these clocks have relied on
437 bisulfite-based assays that provide single CpG resolution [4-11, 64, 65]. These existing clocks
438 rarely share CpGs in common. For instance, a comparison of the three mouse clocks showed
439 only two CpGs in common between the blood-based and multi-tissue clocks [7, 8, 41]. This is
440 not particularly surprising given that these were constructed from reduced representation
441 bisulfite sequencing (RRBS) data, a protocol for which CpG coverage can have low overlap
442 between libraries. But even in the case of the human clocks that were built from microarray
443 data with fixed and limited number of CpGs to select from, the overlap is still poor. The Horvath

444 and Hannum clocks share only about six CpGs in common. This means that DNAmAge can be
445 defined and calibrated from numerous different subsets of potential clock CpGs [9, 41].

446 While MBD-sequencing does not provide single CpG resolution, it is nonetheless known to
447 deliver highly sensitive and reliable quantification of genome-wide methylation [34-36, 39].
448 Instead of measuring individual CpGs, MBD-seq quantifies methylation levels within
449 circumscribed regions containing spatially proximal CpGs that are generally correlated in
450 methylation patterns [66-68]. To test feasibility, we started by training to chronological age
451 using linear regression. Despite the extremely humble sample number, the estimated age had a
452 near perfect correlation with chronological age in the training set (r = 0.99). In the test set of 23
453 mice, the age correlation was at 0.74 with a fairly high median error of ± 90 days. While not
454 precise, this DNAmAge estimator, consisting of 60 clock CpG regions, could still be applied to
455 classify mice into broad age groups (young, middle, old), and may perform just as well as
456 transcriptomic age-classifiers that have been defined from much larger sample numbers [69,
457 70]. The constituent clock CpG regions included sites in or near 29 genes that were represented
458 among the age-DMRs (e.g., *Cyp46a1*, *Fzd8*, *Gata6*), although in terms of the exact CpG regions,
459 only 15 age-DMRs were present in both lists (see **Table S5**). The RRBS-based clock published by
460 Wang et al. [10] was for the liver tissue, and we compared the genes in their list of 149 clock
461 CpGs and we found two common genes, *Cyp46a1* and *Sulf2*, represented in both, although
462 again, the precise CpGs did not overlap.

463 We also applied a direct weighted averaging method that did not impose a training step. Both
464 versions of the age-DMR based clocks (i.e., one built using the full set of 500 age-DMRs, and

465 another built from a restricted set of only 56 lifespan-age-DMRS) provided fairly close estimates
466 of chronological ages. Of these two DNAmAge estimators, only the DNAmAge_56 appeared
467 sensitive to lifespan variability, and the age acceleration derived from this clock was predictive
468 of strain lifespan, and also accelerated in the HFD group. Using this clock, almost all cases from
469 strain-diet groups classified as long-lived had negative DNAmAge-acc; the only exceptions were
470 four F1 samples, including the male B6D2F1, that had positive DNAmAge-acc. For cases
471 belonging to strain-diet groups classified as short-lived, all had positive DNAmAge-acc with the
472 exception of one BXD65 kept on HFD that had negative DNAmAge-acc. The strain with the most
473 decelerated clock, and presumably slowest rate of biological aging, was BXD102 on CD, which is
474 also the longest lived BXD strain we had in the study (**Table 1**). For these mice, the DNAmAge-
475 acc for the female were highly decelerated and ranged from –127 to –194 days. Interestingly,
476 the one male BXD102 had a less decelerated clock with a DNAmAge-acc of –56 days.

477 The members of the DNAmAge_56 clock were selected because these CpGs were both
478 correlates of age, and predictive of lifespan. The majority of these (31 of the 56) were age-
479 hypermethylated and had lower methylation among the long-lived strains (lower right box of
480 **Fig. 7a**). These CpGs also had the most pronounced association with both age and lifespan and
481 were CpGs in the introns, exons and promoters of genes such as *Jak3*, *Wnt5a*, *Abca7* and
482 *Cyp46a1*. The relation between the regression coefficients for age and lifespan would suggest
483 that for these CpGs that gain methylation with age, the long-lived strains have a more
484 "youthful" profile, i.e., lower average methylation. However, 16 of the age-lifespan-DMRs were
485 age-hypomethylated, and yet had lower methylation among the long-lived strains (lower left
486 box of **Fig. 7a**). A few epidemiological studies have also attempted to define predictors of all-

487 cause mortality risk in humans, and these studies paint a very complex picture for humans.
488 While two of the studies showed that hypomethylation at specific CpGs was prognostic of poor
489 survival [71, 72], another study found a combination of both hypo- and hyper-methylated CpGs
490 linked to mortality [73]. A complication with the human studies is that several of the mortality
491 CpGs were also markers for tobacco use, indicating that a good proportion of the CpGs were
492 likely capturing the effects of lifestyle and environmental exposures [72, 74, 75]. In the BXDs,
493 given the controlled environment, the CpG methylation patterns are presumably providing a
494 closer marker of genetic and epigenetic predisposition to life expectancy.

495 Body weight, DNA methylation, and lifespan prediction

496 We also explored a less conventional clock based on the methylation levels at the top 500 BW0-
497 DMRs. This clock does not qualify as a DNAmAge clock since the estimates were uncorrelated
498 with chronological age. Instead, the estimates were correlated with strain longevity data and
499 we tentatively refer to this as lifespan clock (BW0.lifespan clock). The main mismatches
500 between the lifespan predicted by the BW0.lifespan clock versus the recorded strain lifespans
501 were for the long-lived F1 hybrids and BXD65, members of the BXD panel that, in this particular
502 cohort, also exhibited higher body weight. For these F1s and strain, recorded median lifespans
503 are over 790 days; the BW0.lifespan clock incorrectly predicted much shorter lifespans for
504 these cases (all at under 566 days). We note that the simple averages for the top 500 BW0-
505 DMRs (i.e., not weighed by any variable) were also correlated with lifespan but to a lesser
506 degree ($r = -0.41$, $p = 0.0004$). Incorporating the age information by using the age regression

507 coefficients as weighing variables enhanced the predictive power and made it a directly
508 comparable to the lifespan data.

509 A key point of distinction between the DNAmAge and BW0.lifespan clocks is that the DNAmAge
510 is primarily an estimate of chronological age, and the age acceleration is a secondary derivative.
511 The higher DNAmAge-acc in the HFD group also implied that the rate of the clock, as measured
512 by the DNAmAge_56 clock, is a modifiable outcome. The BW0.lifespan clock on the other hand,
513 provided a direct estimate of expected lifespan dependent on a phenotype from a younger age.
514 One could speculate that the BW0.lifespan clock represents a genotype dependent "lifespan
515 potential", while the DNAmAge-acc represents a health-related trait that can be accelerated or
516 decelerated over the course of life, and is responsive to health promoting interventions. This
517 distinction aside, the DNAmAge and the BW0.lifespan clocks had consistent associations with
518 body weight. Specifically, DNAmAge-acc derived from both the 500 and 56 age-DMR clocks
519 showed positive correlation with baseline body weight indicating more accelerated aging for
520 mice with higher body mass. For the BW0.lifespan clock, the estimates were negatively
521 correlated with body weight, also indicating shorter lifespan for mice with higher body mass.
522 This conveys remarkably close interrelations among body weight/mass, the aging methylome
523 and final lifespan. The influence of body mass on longevity and the more favorable health
524 profile associated with smaller body mass has been known for a long time [76-81]. The results
525 we present are further evidence that the epigenome plays a mechanistic intermediary role that
526 links body weight to the rate of biological aging, and the DNA methylation clocks likely capture
527 the effects of weight and other biological factors that collectively influence the longevity of the
528 BXDs.

529 In terms of the direction of causality (i.e., whether the methylome patterns are due to body
530 weight, or body weight differences due to DMRs), based on the timeline of data collection, a
531 simple inference would be that the baseline body weight predicted the methylome patterns
532 and the epigenetic age acceleration. In humans, differences in DNA methylation also appear to
533 be more the effect of, rather that the cause for differences in body mass index [82]. However,
534 both body weight and DNA methylation are genetically regulated phenotypes that are tightly
535 interlinked. And in these mice, body weight from young adulthood had a sustained or even
536 lifelong effect of weight measured later in life. This was also true for the few mice that were
537 introduced to HFD as the mice that were heavier at young age, prior to HFD, continued to be
538 heavier on HFD, indicating a genetic predisposition to heavier bodies. Given this, we are
539 inclined to interpret that these three phenotypic domains (body weight, methylome, longevity)
540 as inter-dependent and are ultimately modulated by underlying DNA sequence variation. A
541 well-powered genetic dissection of these phenotypes will certainly shed more light on the
542 nature of this inter-relatedness.

543 The analysis with the RNA-seq data shows that the aging methylome may have an impact on
544 gene expression. However, the mRNA clocks, derived from much larger sample sizes, had lower
545 correlations with chronological age. Furthermore, the age-accelerations from the two versions
546 of the mRNA clocks had inconsistent associations with body weight, and were not predictive of
547 lifespan.

548 **Technical considerations and caveats**

549 Before concluding, we should address a few caveats. The sequence alignment was done to the
550 mm10 B6 reference genome, which means that for regions with D2 haplotypes, the sequence
551 differences could compromise alignment. The strong population stratification in the PC plot is
552 likely the result of true quantitative variation in methylation, and also due to a portion of the
553 CpG regions serving as surrogates for underlying genotype [83]. The main methylome-wide
554 analysis we performed was for age, and then baseline body weight. Since age is independent of
555 strain and the different BXDs and lifespan groups were represented across the entire age range,
556 the age-DMRs are expected to be less susceptible to the confounding effect of DNA sequence
557 variants. For body weight, a phenotype that is closely linked to genotype, differential
558 quantification due to sequence effects could be more problematic. To partly control for this, we
559 included the top five PCs in the regression models as these PCs capture a portion of the
560 genotype effects and also possibly other unmeasured confounder variables (e.g., cryptic batch
561 effects, cell composition) [39, 84]. For the top 500 age-DMR, only 71 bins (14%) contained at
562 least one sequence variant and the remaining were monomorphic. This is lower than the 17%
563 of variant containing bins in the background set of 368,300 regions. For the top 500 BW0-
564 DMRs, 139 (27.6%) contained sequence variants, and this higher proportion shows that the
565 BW0-DMRs occur in genomic loci that are variable in the BXD, and some of the differential
566 methylation estimates may be conflated by sequence variants. Nonetheless, the majority of the
567 BW0.DMRs used to estimate the clock by weighing on the age coefficients were devoid of
568 sequence variants.

569 Another weakness to consider is that the present study made use of DNA from frozen liver
570 tissue and does not account for cellular composition. This is an issue that is inherent to

571 epigenomic and transcriptomic data from bulk tissue [85]. While the liver is relatively
572 homogeneous in cellular makeup, at least compared to blood or brain, cellular heterogeneity is
573 still a confounding factor, particularly since this is known to increase with age [53, 85]. For this
574 issue too, incorporating the top PCs in the statistics is an *in silico* method to partly mitigate the
575 confounding effect.

576 Conclusion

577 In conclusion, we have provided a comprehensive description of the aging methylome in a
578 subset of the BXD panel. Our results demonstrate that the DNA methylations based epigenetic
579 clock is sensitive to subtle differences in natural lifespan that arise from common genetic
580 variants. The effect of body mass and other biological and environmental variables on lifespan
581 may also be mechanistically mediated by the methylome.

582 Materials and Methods

583 Sample preparation and high throughput sequencing

584 Liver samples were obtained from the BXD colony maintained at the University of Tennessee
585 Health Science Center (see Roy et al. [28] for details). All animal procedures were in accordance
586 to the protocol approved by the Institutional Animal Care and Use Committee (IACUC) at the
587 University of Tennessee Health Science Center. DNA from liver tissue was extracted using the
588 DNeasy Blood & Tissue Kit from Qiagen. Nucleic acid purity was inspected using a NanoDrop
589 spectrophotometer, and quantified using Qubit fluorometer dsDNA BR Assay. Affinity based

590 enrichment was carried out using the MethylMiner DNA enrichment kit from ThermoFisher
591 Scientific according to the standard manufacturer's protocol. This kit relies on the methyl-CpG
592 binding domain (MBD) protein to capture methylated CpG fragments. In brief, 1 µg of DNA in
593 110 µl of low TE buffer was fragmented to ~150 bp using a Covaris S2 ultrasonicator. The
594 sonication settings were: cycle/burst of 1 for 10 cycles of 60 s, duty cycle of 10%, intensity of
595 5.0. DNA fragment size and quality were assessed using the Agilent Bioanalyzer 2100. Following
596 the MBD capture reactions, DNA was eluted in a single step using the high salt (2000 mM NaCl)
597 elution buffer, and re-concentrated by ethanol precipitation. The final concentration of
598 methylated-CpG enriched DNA ranged from 1.12 to 5.43 ηg per µl (2.46 ± 0.94). The library
599 construction and sequencing were carried out at Novogene Genomic Services facility.
600 Sequencing was done to a depth of approximately 50 million reads per sample (150 bp paired-
601 end) on the Illumina HiSeq 4000.

602 Read alignment and data quality

603 The FASTQ files were first inspected with the FastQC tool (v.0.11.8) [86], and all files passed the
604 initial quality checks. Alignment was then done to the mouse reference genome
605 (mm10/GRCm38) using the Bowtie2 aligner (v.2.3.4.3) [87], and alignment quality was
606 evaluated with SAMtools (v.1.9) [88], and SAMstat v.1.5.1[89]. Potential PCR duplicates and
607 reads with mapping quality less than 10 were filtered out, and indexed Bam files were created.
608 The Bam files were then loaded to the MEDIPS R package (v.1.36.0) [90], for additional quality
609 control and assessment of read coverage. Saturation analysis (MEDIPS.saturation) showed that
610 all 70 libraries had sufficient read coverage, and pair-wise correlations (MEDIPS.correlation)

611 showed high consistency between samples (Pearson $r > 0.90$ for all pairs). Given the MBD
612 enrichment, all the samples were enriched for CpGs (mean CG enrichment score of 2.30 ± 0.19;
613 using the MEDIPS MEDIPS.CpGenrich function), and on average, 51% of CpGs in the reference
614 genome was covered by at least one mapped read, with 28% of CpGs covered by > 5 mapped
615 reads. To quantify DNA methylation, the mouse genome was divided in 150 bp non-overlapping
616 windows and reads were counted for each bin with normalization to the local CpG density
617 (referred to as coupling factor or CF) using the function MEDIPS.meth and the following
618 parameters: ws =150, extend = 150, uniq = 1, shift=0.

619 **Global methylome analysis**

620 Read counts generated in MEDIPS were filtered to retain only the 150 bp bins that had
621 sufficient coverage for reliable quantification and statistical analyses. First, bins with no CpGs
622 (CF = 0) and mean read counts ≤ 1 were excluded, resulting in 4,286,826 bins. The Y
623 chromosome was also excluded. Following these filters, the data was loaded to the EdgeR R
624 package (v3.24) [91] and further filtered on the basis of counts per million (CPM) such than only
625 reads with more than 1 count per million in 2 or more libraries were retained. This resulted in
626 368,300 CpG regions with sufficient coverage across the libraries, these were normalized using
627 the calcNormFactors in EdgeR, and RPKM values extracted using the parameters gene.length =
628 150, log = TRUE. These 368,300 bins had a mean CpG density of 5.4 ± 2.6 and in total cover
629 2,001,723 CpG sites. The compendium of SNPs and small insertions/deletions segregating in the
630 BXDs have been catalogued for the BXDs [92, 93], and we used this information to count the
631 number of variants in each of the 368,300 150 bp bins.

632 To evaluate sample clustering and to detect potential outliers, we performed PCA and
633 hierarchical clustering (**Fig. S1a**). There were no outlier samples and the DNA methylation
634 profile was highly consistent across the samples (**Fig. S1b**) and averaged at 3.8 ± 0.72 logRPKM.
635 These CpG regions were then annotated for genomic features using the HOMER program
636 (v4.10) [94] and evaluated for enrichment relative to the genome-wide set using a
637 hypergeometric test (R codes in **Table S2**). Based on the annotations, the CpG regions were
638 then divided into bins that occurred within annotated genes (genic set, 200531 bins), and those
639 that were in intergenic regions (167769 bins). For each sample, the overall average methylation
640 and variance for these genic and intergenic sets were computed. The intercorrelations between
641 the large-scale methylome features, body weight measures, and strain-level lifespan phenotype
642 were examined using Pearson correlations.

643 **Statistics for differential methylation analyses**

644 To detect age-DMRs, we applied a generalized multiple regression model that included diet and
645 the top 5 PCs: glm(logRPKM ~ age + diet + PC1 + PC2 + PC3 + PC4 + PC5). The top 5 PCs were
646 included so that the age-effect can be adjusted for other major sources of variance, including
647 strain effect and other unmeasured potential confounder variables. The top age-DMRs were
648 selected at a lenient statistical threshold of unadjusted $p \leq 3.1 \times 10^{-4}$ (23% FDR) since our
649 primary goal was to examine the overall trends and to test if these sites can collectively be used
650 to estimate chronological age and lifespan prediction. For these, GSEA was carried out using the
651 WebGestalt platform (http://www.webgestalt.org) with genes ranked by the age regression
652 coefficients [95, 96]. To test if the top 500 age-DMRs were associated with strain-level lifespan,

653 we applied a mixed effects model using the lme4 R package (v4_1.1-19) [97]. The lifespan data
654 are at the level of strain within a diet group (CD or HFD), and to test association between the
655 individual level DNA methylation and the strain-diet longevity data, we treated strain-diet as a
656 random variable. The mixed effects model was: lmer(logRPKM ~ age + median.lifespan + (1 +
657 age|strain.diet)), where age and median lifespan are numeric variables and strain.diet is a
658 categorical identity. To identify CpG regions that are associated with baseline body weight
659 variation, we used the regression model: glm(logRPKM ~ BW0 + age + PC1 + PC2 + PC3 + PC4 +
660 PC5), where BW0 was baseline body weight as a numeric variable.

661 Epigenetic clock calculation

662 For the training-based clock construction, we applied elastic net regression (alpha=0.5 using the
663 glmnet R package (v2.0-18) [98, 99]. For the DNA methylation data, we randomly selected 36 of
664 the 69 samples as a training set, and training was done using the log RPKM values for the
665 368,300 CpG bins. The untransformed chronological age of mice in days was entered as the
666 training variable. Model parameters were optimized using a 10-fold cross-validation with the
667 following cv.glmnet parameter: nfolds = 50, alpha = 0,5, family ="gaussian". The performance of
668 the age estimator were then tested in the remaining 33 MBD-seq samples. The accuracy of the
669 predicted age was examined by Pearson correlation with chronological age. As a second
670 measure of accuracy, we also used the median absolute error as described in Horvath & Raj
671 [40]. As recommended in Thompson et al. 2018 [9], the "age acceleration" was computed as
672 the residuals after fitting the predicted age to chronological ages: residuals(lm(DNAmAge ~
673 Age)).

674 For non-training DNA methylation clocks, each CpG region was weighed by the age regression
675 coefficient derived from the equation: glm(logRPKM ~ age + diet + PC1 + PC2 + PC3 + PC4 +
676 PC5), which means that each CpG region was weighed by the change in DNA methylation per
677 unit change in age. For the for the 500 age-DMR version, the weighted average was computed
678 for the 500 CpG regions; for the 56 lifespan-age-DMR version, the weighted averages were
679 computed from the restricted set of 56 CpG regions (for each CpG region, the weighing factor is
680 in the Estimate.Age column of **Table 54**). The DNAmAge_56 and DNAmAge_500 clocks were
681 then derived by scaling the weighted average to the age scale in the 69 samples using the
682 following formula: DNAmAge = (((weighted.average – min.weighted.average) x age.range) /
683 weighted.average.range) + min.age, where min.weighted.average and weighted.average.range
684 are the minimum value and range for the weighted averages in the 69 BXD samples, and
685 age.range = 578 days is the range of chronological age in the 69 BXDs, and min.age = 181 days is
686 the minimum age for the 69 BXDs. For the body weighted based clock, we again used the age
687 coefficient from the same regression model as a weighing factor, but the weighted averages
688 were computed for the top 500 CpG regions that were associated significantly with baseline
689 body weight of mice. The same scaling formula was applied to bring the weighted averages to
690 the same scale the median lifespan data.

691 **Transcriptomes analyses**

692 We used liver gene expression data from a larger cohort of 291 BXDs that is available from
693 GeneNetwork 2 [100]. The RNA sequencing was carried out in two batches, with batch 1
694 generated in 2017 from 150 samples (77 CD and 73 HFD cases), and batch 2 generated in 2018

695 from another set of 141 samples (84 CD and 57 HFD). While the liver specimens all came from
696 the UTHSC Aging BXD Colony, the two batches did not share overlapping samples. Batch 2 had
697 lower sequencing depth than batch 1, and to make the two batches more comparable, we
698 excluded all transcripts with no read coverage (i.e., logRPKM values of 0) in 10% or more of the
699 291 samples, and this retained 25,676 Ensemble transcript IDs. The 347 age-DMR genes were
700 matched by gene symbol to the corresponding transcripts, and only 265 of the age-DMR genes
701 paired to one or more transcript variants in the liver transcriptome. We performed a simple
702 Pearson correlation between the expression of these transcripts and age using data from both
703 batches. In the case of age-DMR genes that matched to multiple transcript variants (specifically,
704 different Ensemble transcript variants) from the same gene, we retained only the transcript
705 with the most significant correlation with age that resulted in 265 unique age-DMR and mRNA
706 pairs (**Table S9**).

707 For mRNA based age estimation, we considered the 25,676 transcripts and applied the same
708 elastic net regression parameters as described for the DNA methylation clocks. In the case of
709 the RNA-seq data, the training to age was first carried out in the 150 cases from batch 1,
710 followed by validation in the 141 cases from batch 2. This was then complemented by
711 performing the training in the 141 cases from batch 2, followed by validate in batch 1.

712 Data availability

713 The normalized MBD-seq data for the 368,300 CpG bins that were considered for statistical
714 analyses and sample metadata will be available from the NCBI NIH Gene Expression

715 Omnibus upon official publication. The full raw alignment files for the MBD-seq data will be

716 made available from the NCBI NIH Sequence Repository Archive upon official publication.

717 Abbreviations

718 age-DMR: age-associated Differentially Methylation Region

719 bp: base pair

720 BW0-DMR: Baseline body Weight associated differentially methylated CpG region

721 BW0: Baseline body Weight

722 BW0.lifespan: baseline weight-based lifespan clock

723 CD: Control Diet

724 CF: Coupling Factor

725 CPM: Counts Per Million

726 DNAmAge-acc: DNA methylation age acceleration

727 DNAmAge: DNA methylation age

728 GO: Gene Ontology

729 GSEA: Gene Set Enrichment Analysis

730 HFD: High Fat Diet

731 KEGG: Kyoto Encyclopedia of Genes and Genomes

732 MBD-seq: Methyl-CpG binding domain sequencing

733 mRNAage: mRNA based age estimates

734 RRBS: Reduced Representation Bisulfite Sequencing

735 PC: Principal Component

736 PCA: Principal Component Analysis

737 QC: Quality Control

738 RPKM: Reads Per Kilo base per Million mapped reads

739 SNP: Single Nucleotide Polymorphism

740

741 ## Declarations

742 **Ethics approval and consent to participate.** All animal procedures were in accordance to

743 protocol approved by the Institutional Animal Care and Use Committee (IACUC) at the

744 University of Tennessee Health Science Center.

745 **Consent for publication.** All author read and approved the current version of the manuscript

746 **Availability of data and materials.** The normalized data and the raw fastq files will be made

747 available from NCBI NIH Gene Expression Omnibus and the Sequence Repository Archive upon

748 official publication.

749 **Competing interests.** No competing interests

750 **Funding:** Funded by NIH NIA grants R21AG055841 and R01AG043930

751 **Authors' contributions**

752 KM supervised the study, contributed to conception of study design and analysis, and wrote the

753 manuscript. RWW contributed to the conception of the BXD Aging Colony, and provided access

754 to the biorepository resource. JVSS, AHBH, and EGW contributed to the lab work, and JVSS

755 performed the primary bioinformatics and contributed to analysis and manuscript. DA and SR

756 contributed to analysis and data acquisition. All authors contributed to and approved the final

757 version of the manuscript.

758 ## Acknowledgements

759 The present work relied on resources from the BXD Aging Colony, and we thank the entire
760 team, particularly Dr. Lu Lu, Jesse Ingels, Casey J Chapman, Melinda S McCarty, Megan K
761 Mulligan, and Arthur Centeno. We thank Dr. Saunak Sen for his invaluable comments of the
762 statistics. We thank the UTHSC-Rhodes College Population Health Researcher Program and Dr.
763 Teresa Waters for support and for bringing an excellent summer student to the PI's lab. We
764 thank Dr. Karolina A. Aberg and her team at the Virginia Commonwealth University for their
765 advice on the MBD-seq technique.

766 ## References.

767 1. Marioni RE, Harris SE, Shah S, McRae AF, von Zglinicki T, Martin-Ruiz C, et al. The
768 epigenetic clock and telomere length are independently associated with chronological age and
769 mortality. International journal of epidemiology. 2018;47(1):356. Epub 2017/12/01. doi:
770 10.1093/ije/dyx233. PubMed PMID: 29190382; PubMed Central PMCID: PMCPMC5837660.
771 2. Mitteldorf J. An epigenetic clock controls aging. Biogerontology. 2016;17(1):257-65.
772 Epub 2015/11/27. doi: 10.1007/s10522-015-9617-5. PubMed PMID: 26608516.
773 3. Lowe D, Horvath S, Raj K. Epigenetic clock analyses of cellular senescence and ageing.
774 Oncotarget. 2016;7(8):8524-31. PubMed PMID: WOS:000375618100007.
775 4. Hannum G, Guinney J, Zhao L, Zhang L, Hughes G, Sadda S, et al. Genome-wide
776 methylation profiles reveal quantitative views of human aging rates. Molecular cell.
777 2013;49(2):359-67. doi: 10.1016/j.molcel.2012.10.016. PubMed PMID: 23177740; PubMed
778 Central PMCID: PMC3780611.
779 5. Horvath S. DNA methylation age of human tissues and cell types. Genome biology.
780 2013;14(10):R115. doi: 10.1186/gb-2013-14-10-r115. PubMed PMID: 24138928; PubMed
781 Central PMCID: PMC4015143.
782 6. Levine ME, Lu AT, Quach A, Chen BH, Assimes TL, Bandinelli S, et al. An epigenetic
783 biomarker of aging for lifespan and healthspan. Aging. 2018;10(4):573-91. Epub 2018/04/21.
784 doi: 10.18632/aging.101414. PubMed PMID: 29676998; PubMed Central PMCID:
785 PMCPMC5940111.
786 7. Petkovich DA, Podolskiy DI, Lobanov AV, Lee SG, Miller RA, Gladyshev VN. Using DNA
787 Methylation Profiling to Evaluate Biological Age and Longevity Interventions. Cell metabolism.
788 2017;25(4):954-60 e6. Epub 2017/04/06. doi: 10.1016/j.cmet.2017.03.016. PubMed PMID:
789 28380383; PubMed Central PMCID: PMCPMC5578459.

790 8. Stubbs TM, Bonder MJ, Stark AK, Krueger F, Team BIAC, von Meyenn F, et al. Multi-
791 tissue DNA methylation age predictor in mouse. Genome biology. 2017;18(1):68. doi:
792 10.1186/s13059-017-1203-5. PubMed PMID: 28399939; PubMed Central PMCID: PMC5389178.
793 9. Thompson MJ, Chwialkowska K, Rubbi L, Lusis AJ, Davis RC, Srivastava A, et al. A multi-
794 tissue full lifespan epigenetic clock for mice. Aging. 2018;10(10):2832-54. Epub 2018/10/24.
795 doi: 10.18632/aging.101590. PubMed PMID: 30348905; PubMed Central PMCID:
796 PMCPMC6224226.
797 10. Wang T, Tsui B, Kreisberg JF, Robertson NA, Gross AM, Yu MK, et al. Epigenetic aging
798 signatures in mice livers are slowed by dwarfism, calorie restriction and rapamycin treatment.
799 Genome biology. 2017;18(1):57. Epub 2017/03/30. doi: 10.1186/s13059-017-1186-2. PubMed
800 PMID: 28351423; PubMed Central PMCID: PMCPMC5371228.
801 11. Weidner CI, Lin Q, Koch CM, Eisele L, Beier F, Ziegler P, et al. Aging of blood can be
802 tracked by DNA methylation changes at just three CpG sites. Genome biology. 2014;15(2):R24.
803 doi: 10.1186/gb-2014-15-2-r24. PubMed PMID: 24490752; PubMed Central PMCID:
804 PMC4053864.
805 12. Marioni RE, Shah S, McRae AF, Chen BH, Colicino E, Harris SE, et al. DNA methylation age
806 of blood predicts all-cause mortality in later life. Genome biology. 2015;16(1):25. doi:
807 10.1186/s13059-015-0584-6. PubMed PMID: 25633388; PubMed Central PMCID: PMC4350614.
808 13. Chen BH, Marioni RE, Colicino E, Peters MJ, Ward-Caviness CK, Tsai PC, et al. DNA
809 methylation-based measures of biological age: meta-analysis predicting time to death. Aging.
810 2016;8(9):1844-65. Epub 2016/10/01. doi: 10.18632/aging.101020. PubMed PMID: 27690265;
811 PubMed Central PMCID: PMCPMC5076441.
812 14. Zhang Y, Hapala J, Brenner H, Wagner W. Individual CpG sites that are associated with
813 age and life expectancy become hypomethylated upon aging. Clinical epigenetics. 2017;9. doi:
814 ARTN 9
815 10.1186/s13148-017-0315-9. PubMed PMID: WOS:000393925000001.
816 15. Christiansen L, Lenart A, Tan Q, Vaupel JW, Aviv A, McGue M, et al. DNA methylation
817 age is associated with mortality in a longitudinal Danish twin study. Aging cell. 2016;15(1):149-
818 54. Epub 2015/11/26. doi: 10.1111/acel.12421. PubMed PMID: 26594032; PubMed Central
819 PMCID: PMCPMC4717264.
820 16. Lin Q, Weidner CI, Costa IG, Marioni RE, Ferreira MRP, Deary IJ, et al. DNA methylation
821 levels at individual age-associated CpG sites can be indicative for life expectancy. Aging-Us.
822 2016;8(2):394-401. doi: DOI 10.18632/aging.100908. PubMed PMID: WOS:000372086600017.
823 17. Marioni RE, Shah S, McRae AF, Ritchie SJ, Muniz-Terrera G, Harris SE, et al. The
824 epigenetic clock is correlated with physical and cognitive fitness in the Lothian Birth Cohort
825 1936. International journal of epidemiology. 2015;44(4):1388-96. doi: 10.1093/ije/dyu277.
826 PubMed PMID: 25617346; PubMed Central PMCID: PMC4588858.
827 18. Perna L, Zhang Y, Mons U, Holleczek B, Saum KU, Brenner H. Epigenetic age acceleration
828 predicts cancer, cardiovascular, and all-cause mortality in a German case cohort. Clinical
829 epigenetics. 2016;8:64. Epub 2016/06/09. doi: 10.1186/s13148-016-0228-z. PubMed PMID:
830 27274774; PubMed Central PMCID: PMCPMC4891876.
831 19. Lowe R, Barton C, Jenkins CA, Ernst C, Forman O, Fernandez-Twinn DS, et al. Ageing-
832 associated DNA methylation dynamics are a molecular readout of lifespan variation among

833 mammalian species. Genome biology. 2018;19(1):22. Epub 2018/02/18. doi: 10.1186/s13059-
834 018-1397-1. PubMed PMID: 29452591; PubMed Central PMCID: PMCPMC5815211.
835 20. Cole JJ, Robertson NA, Rather MI, Thomson JP, McBryan T, Sproul D, et al. Diverse
836 interventions that extend mouse lifespan suppress shared age-associated epigenetic changes at
837 critical gene regulatory regions. Genome biology. 2017;18. doi: ARTN 58
838 10.1186/s13059-017-1185-3. PubMed PMID: WOS:000397557000003.
839 21. Hahn O, Gronke S, Stubbs TM, Ficz G, Hendrich O, Krueger F, et al. Dietary restriction
840 protects from age-associated DNA methylation and induces epigenetic reprogramming of lipid
841 metabolism. Genome biology. 2017;18(1):56. Epub 2017/03/30. doi: 10.1186/s13059-017-
842 1187-1. PubMed PMID: 28351387; PubMed Central PMCID: PMCPMC5370449.
843 22. Sziraki A, Tyshkovskiy A, Gladyshev VN. Global remodeling of the mouse DNA
844 methylome during aging and in response to calorie restriction. Aging cell. 2018;17(3):e12738.
845 Epub 2018/03/27. doi: 10.1111/acel.12738. PubMed PMID: 29575528; PubMed Central PMCID:
846 PMCPMC5946071.
847 23. Hook M, Roy S, Williams EG, Bou Sleiman M, Mozhui K, Nelson JF, et al. Genetic
848 cartography of longevity in humans and mice: Current landscape and horizons. Biochimica et
849 biophysica acta. 2018. Epub 2018/02/08. doi: 10.1016/j.bbadis.2018.01.026. PubMed PMID:
850 29410319.
851 24. de Haan G, Gelman R, Watson A, Yunis E, Van Zant G. A putative gene causes variability
852 in lifespan among genotypically identical mice. Nature genetics. 1998;19(2):114-6. doi:
853 10.1038/465. PubMed PMID: 9620762.
854 25. De Haan G, Van Zant G. Genetic analysis of hemopoietic cell cycling in mice suggests its
855 involvement in organismal life span. FASEB journal : official publication of the Federation of
856 American Societies for Experimental Biology. 1999;13(6):707-13. PubMed PMID: 10094931.
857 26. Gelman R, Watson A, Bronson R, Yunis E. Murine chromosomal regions correlated with
858 longevity. Genetics. 1988;118(4):693-704. PubMed PMID: 3163317; PubMed Central PMCID:
859 PMC1203324.
860 27. Lang DH, Gerhard GS, Griffith JW, Vogler GP, Vandenbergh DJ, Blizard DA, et al.
861 Quantitative trait loci (QTL) analysis of longevity in C57BL/6J by DBA/2J (BXD) recombinant
862 inbred mice. Aging clinical and experimental research. 2010;22(1):8-19. PubMed PMID:
863 20305363.
864 28. Roy S, Sleiman MB, Jha P, Williams EG, Ingels JF, Chapman CJ, et al. Modulation of
865 longevity by diet, and youthful body weight, but not by weight gain after maturity. bioRxiv.
866 2019:776559. doi: 10.1101/776559.
867 29. Yuan R, Peters LL, Paigen B. Mice as a mammalian model for research on the genetics of
868 aging. ILAR journal / National Research Council, Institute of Laboratory Animal Resources.
869 2011;52(1):4-15. PubMed PMID: 21411853; PubMed Central PMCID: PMC3074346.
870 30. Yuan R, Tsaih SW, Petkova SB, Marin de Evsikova C, Xing S, Marion MA, et al. Aging in
871 inbred strains of mice: study design and interim report on median lifespans and circulating IGF1
872 levels. Aging cell. 2009;8(3):277-87. doi: 10.1111/j.1474-9726.2009.00478.x. PubMed PMID:
873 19627267; PubMed Central PMCID: PMC2768517.
874 31. Hsu HC, Li L, Zhang HG, Mountz JD. Genetic regulation of thymic involution. Mechanisms
875 of ageing and development. 2005;126(1):87-97. doi: 10.1016/j.mad.2004.09.016. PubMed
876 PMID: 15610766.

877 32. Sloane LB, Stout JT, Austad SN, McClearn GE. Tail tendon break time: a biomarker of
878 aging? The journals of gerontology Series A, Biological sciences and medical sciences.
879 2011;66(3):287-94. doi: 10.1093/gerona/glq196. PubMed PMID: 21059835; PubMed Central
880 PMCID: PMC3041475.
881 33. Sloane LB, Stout JT, Vandenbergh DJ, Vogler GP, Gerhard GS, McClearn GE. Quantitative
882 trait loci analysis of tail tendon break time in mice of C57BL/6J and DBA/2J lineage. The journals
883 of gerontology Series A, Biological sciences and medical sciences. 2011;66(2):170-8. doi:
884 10.1093/gerona/glq169. PubMed PMID: 21047976; PubMed Central PMCID: PMC3021371.
885 34. Aberg KA, Xie L, Chan RF, Zhao M, Pandey AK, Kumar G, et al. Evaluation of Methyl-
886 Binding Domain Based Enrichment Approaches Revisited. PloS one. 2015;10(7):e0132205. doi:
887 10.1371/journal.pone.0132205. PubMed PMID: 26177298; PubMed Central PMCID:
888 PMC4503759.
889 35. Aberg KA, McClay JL, Nerella S, Xie LY, Clark SL, Hudson AD, et al. MBD-seq as a cost-
890 effective approach for methylome-wide association studies: demonstration in 1500 case--
891 control samples. Epigenomics. 2012;4(6):605-21. doi: 10.2217/epi.12.59. PubMed PMID:
892 23244307; PubMed Central PMCID: PMC3923085.
893 36. Aberg KA, Chan RF, Xie L, Shabalin AA, van den Oord E. Methyl-CpG-Binding Domain
894 Sequencing: MBD-seq. Methods in molecular biology. 2018;1708:171-89. Epub 2017/12/11.
895 doi: 10.1007/978-1-4939-7481-8_10. PubMed PMID: 29224145.
896 37. GeneNetwork 2. Available from: http://gn2.genenetwork.org.
897 38. Johansson A, Enroth S, Gyllensten U. Continuous Aging of the Human DNA Methylome
898 Throughout the Human Lifespan. PloS one. 2013;8(6):e67378. doi:
899 10.1371/journal.pone.0067378. PubMed PMID: 23826282; PubMed Central PMCID:
900 PMC3695075.
901 39. McClay JL, Aberg KA, Clark SL, Nerella S, Kumar G, Xie LY, et al. A methylome-wide study
902 of aging using massively parallel sequencing of the methyl-CpG-enriched genomic fraction from
903 blood in over 700 subjects. Human molecular genetics. 2014;23(5):1175-85. doi:
904 10.1093/hmg/ddt511. PubMed PMID: 24135035; PubMed Central PMCID: PMC3919012.
905 40. Horvath S, Raj K. DNA methylation-based biomarkers and the epigenetic clock theory of
906 ageing. Nature reviews Genetics. 2018;19(6):371-84. Epub 2018/04/13. doi: 10.1038/s41576-
907 018-0004-3. PubMed PMID: 29643443.
908 41. Field AE, Robertson NA, Wang T, Havas A, Ideker T, Adams PD. DNA Methylation Clocks
909 in Aging: Categories, Causes, and Consequences. Molecular cell. 2018;71(6):882-95. Epub
910 2018/09/23. doi: 10.1016/j.molcel.2018.08.008. PubMed PMID: 30241605.
911 42. Bacalini MG, Franceschi C, Gentilini D, Ravaioli F, Zhou X, Remondini D, et al. Molecular
912 Aging of Human Liver: An Epigenetic/Transcriptomic Signature. The journals of gerontology
913 Series A, Biological sciences and medical sciences. 2019;74(1):1-8. Epub 2018/03/20. doi:
914 10.1093/gerona/gly048. PubMed PMID: 29554203.
915 43. Snir S, Farrell C, Pellegrini M. Human epigenetic ageing is logarithmic with time across
916 the entire lifespan. Epigenetics : official journal of the DNA Methylation Society.
917 2019;14(9):912-26. doi: 10.1080/15592294.2019.1623634. PubMed PMID:
918 WOS:000479080700005.

919 44. Ciccarone F, Tagliatesta S, Caiafa P, Zampieri M. DNA methylation dynamics in aging:
920 how far are we from understanding the mechanisms? Mechanisms of ageing and development.
921 2018;174:3-17. Epub 2017/12/23. doi: 10.1016/j.mad.2017.12.002. PubMed PMID: 29268958.
922 45. Zampieri M, Ciccarone F, Calabrese R, Franceschi C, Burkle A, Caiafa P. Reconfiguration
923 of DNA methylation in aging. Mechanisms of ageing and development. 2015;151:60-70. doi:
924 10.1016/j.mad.2015.02.002. PubMed PMID: 25708826.
925 46. Heyn H, Li N, Ferreira HJ, Moran S, Pisano DG, Gomez A, et al. Distinct DNA methylomes
926 of newborns and centenarians. Proceedings of the National Academy of Sciences of the United
927 States of America. 2012;109(26):10522-7. doi: 10.1073/pnas.1120658109. PubMed PMID:
928 22689993; PubMed Central PMCID: PMC3387108.
929 47. Maegawa S, Hinkal G, Kim HS, Shen L, Zhang L, Zhang J, et al. Widespread and tissue
930 specific age-related DNA methylation changes in mice. Genome research. 2010;20(3):332-40.
931 doi: 10.1101/gr.096826.109. PubMed PMID: 20107151; PubMed Central PMCID: PMC2840983.
932 48. Unnikrishnan A, Hadad N, Masser DR, Jackson J, Freeman WM, Richardson A. Revisiting
933 the genomic hypomethylation hypothesis of aging. Annals of the New York Academy of
934 Sciences. 2018;1418(1):69-79. Epub 2018/01/25. doi: 10.1111/nyas.13533. PubMed PMID:
935 29363785.
936 49. Singhal RP, Mays-Hoopes LL, Eichhorn GL. DNA methylation in aging of mice.
937 Mechanisms of ageing and development. 1987;41(3):199-210. Epub 1987/12/01. doi:
938 10.1016/0047-6374(87)90040-6. PubMed PMID: 3431172.
939 50. Cruickshanks HA, McBryan T, Nelson DM, Vanderkraats ND, Shah PP, van Tuyn J, et al.
940 Senescent cells harbour features of the cancer epigenome. Nat Cell Biol. 2013;15(12):1495-506.
941 Epub 2013/11/26. doi: 10.1038/ncb2879. PubMed PMID: 24270890; PubMed Central PMCID:
942 PMCPMC4106249.
943 51. Day K, Waite LL, Thalacker-Mercer A, West A, Bamman MM, Brooks JD, et al. Differential
944 DNA methylation with age displays both common and dynamic features across human tissues
945 that are influenced by CpG landscape. Genome biology. 2013;14(9):R102. Epub 2013/09/17.
946 doi: 10.1186/gb-2013-14-9-r102. PubMed PMID: 24034465; PubMed Central PMCID:
947 PMCPMC4053985.
948 52. Rakyan VK, Down TA, Maslau S, Andrew T, Yang TP, Beyan H, et al. Human aging-
949 associated DNA hypermethylation occurs preferentially at bivalent chromatin domains.
950 Genome research. 2010;20(4):434-9. Epub 2010/03/12. doi: 10.1101/gr.103101.109. PubMed
951 PMID: 20219945; PubMed Central PMCID: PMCPMC2847746.
952 53. Teschendorff AE, Menon U, Gentry-Maharaj A, Ramus SJ, Weisenberger DJ, Shen H, et
953 al. Age-dependent DNA methylation of genes that are suppressed in stem cells is a hallmark of
954 cancer. Genome research. 2010;20(4):440-6. doi: 10.1101/gr.103606.109. PubMed PMID:
955 20219944; PubMed Central PMCID: PMC2847747.
956 54. Carter CJ. Convergence of genes implicated in Alzheimer's disease on the cerebral
957 cholesterol shuttle: APP, cholesterol, lipoproteins, and atherosclerosis. Neurochem Int.
958 2007;50(1):12-38. Epub 2006/09/16. doi: 10.1016/j.neuint.2006.07.007. PubMed PMID:
959 16973241.
960 55. Steinberg S, Stefansson H, Jonsson T, Johannsdottir H, Ingason A, Helgason H, et al. Loss-
961 of-function variants in ABCA7 confer risk of Alzheimer's disease. Nature genetics.
962 2015;47(5):445-7. Epub 2015/03/26. doi: 10.1038/ng.3246. PubMed PMID: 25807283.

963 56. Sebastiani P, Montano M, Puca A, Solovieff N, Kojima T, Wang MC, et al. RNA editing
964 genes associated with extreme old age in humans and with lifespan in C. elegans. PloS one.
965 2009;4(12):e8210. Epub 2009/12/17. doi: 10.1371/journal.pone.0008210. PubMed PMID:
966 20011587; PubMed Central PMCID: PMCPMC2788130.
967 57. Yashin AI, Wu D, Arbeev KG, Ukraintseva SV. Joint influence of small-effect genetic
968 variants on human longevity. Aging. 2010;2(9):612-20. Epub 2010/09/14. doi:
969 10.18632/aging.100191. PubMed PMID: 20834067; PubMed Central PMCID: PMCPMC2984609.
970 58. Soerensen M, Dato S, Tan Q, Thinggaard M, Kleindorp R, Beekman M, et al. Human
971 longevity and variation in GH/IGF-1/insulin signaling, DNA damage signaling and repair and
972 pro/antioxidant pathway genes: cross sectional and longitudinal studies. Experimental
973 gerontology. 2012;47(5):379-87. Epub 2012/03/13. doi: 10.1016/j.exger.2012.02.010. PubMed
974 PMID: 22406557; PubMed Central PMCID: PMCPMC3334439.
975 59. Dato S, Soerensen M, Montesanto A, Lagani V, Passarino G, Christensen K, et al. UCP3
976 polymorphisms, hand grip performance and survival at old age: association analysis in two
977 Danish middle aged and elderly cohorts. Mechanisms of ageing and development.
978 2012;133(8):530-7. Epub 2012/06/30. doi: 10.1016/j.mad.2012.06.004. PubMed PMID:
979 22743239; PubMed Central PMCID: PMCPMC3629378.
980 60. Slack C, Alic N, Foley A, Cabecinha M, Hoddinott MP, Partridge L. The Ras-Erk-ETS-
981 Signaling Pathway Is a Drug Target for Longevity. Cell. 2015;162(1):72-83. Epub 2015/06/30.
982 doi: 10.1016/j.cell.2015.06.023. PubMed PMID: 26119340; PubMed Central PMCID:
983 PMCPMC4518474.
984 61. Passtoors WM, van den Akker EB, Deelen J, Maier AB, van der Breggen R, Jansen R, et al.
985 IL7R gene expression network associates with human healthy ageing. Immunity & ageing : I & A.
986 2015;12:21. Epub 2015/11/14. doi: 10.1186/s12979-015-0048-6. PubMed PMID: 26566388;
987 PubMed Central PMCID: PMCPMC4642670.
988 62. Zhang G, Li J, Purkayastha S, Tang Y, Zhang H, Yin Y, et al. Hypothalamic programming of
989 systemic ageing involving IKK-beta, NF-kappaB and GnRH. Nature. 2013;497(7448):211-6. Epub
990 2013/05/03. doi: 10.1038/nature12143. PubMed PMID: 23636330; PubMed Central PMCID:
991 PMCPMC3756938.
992 63. Mozhui K, Pandey AK. Conserved effect of aging on DNA methylation and association
993 with EZH2 polycomb protein in mice and humans. Mechanisms of ageing and development.
994 2017;162:27-37. Epub 2017/03/03. doi: 10.1016/j.mad.2017.02.006. PubMed PMID: 28249716;
995 PubMed Central PMCID: PMCPMC5411177.
996 64. Huang Y, Yan J, Hou J, Fu X, Li L, Hou Y. Developing a DNA methylation assay for human
997 age prediction in blood and bloodstain. Forensic Sci Int Genet. 2015;17:129-36. Epub
998 2015/05/17. doi: 10.1016/j.fsigen.2015.05.007. PubMed PMID: 25979242.
999 65. Zbiec-Piekarska R, Spolnicka M, Kupiec T, Parys-Proszek A, Makowska Z, Paleczka A, et
1000 al. Development of a forensically useful age prediction method based on DNA methylation
1001 analysis. Forensic Sci Int Genet. 2015;17:173-9. Epub 2015/06/01. doi:
1002 10.1016/j.fsigen.2015.05.001. PubMed PMID: 26026729.
1003 66. Zhang W, Spector TD, Deloukas P, Bell JT, Engelhardt BE. Predicting genome-wide DNA
1004 methylation using methylation marks, genomic position, and DNA regulatory elements.
1005 Genome biology. 2015;16:14. doi: 10.1186/s13059-015-0581-9. PubMed PMID: 25616342;
1006 PubMed Central PMCID: PMC4389802.

1007 67. Lovkvist C, Dodd IB, Sneppen K, Haerter JO. DNA methylation in human epigenomes
1008 depends on local topology of CpG sites. Nucleic acids research. 2016;44(11):5123-32. doi:
1009 10.1093/nar/gkw124. PubMed PMID: 26932361.
1010 68. Li Y, Zhu J, Tian G, Li N, Li Q, Ye M, et al. The DNA methylome of human peripheral blood
1011 mononuclear cells. PLoS biology. 2010;8(11):e1000533. doi: 10.1371/journal.pbio.1000533.
1012 PubMed PMID: 21085693; PubMed Central PMCID: PMC2976721.
1013 69. Janssens GE, Lin XX, Millan-Arino L, Kavsek A, Sen I, Seinstra RI, et al. Transcriptomics-
1014 Based Screening Identifies Pharmacological Inhibition of Hsp90 as a Means to Defer Aging. Cell
1015 Rep. 2019;27(2):467-80 e6. Epub 2019/04/11. doi: 10.1016/j.celrep.2019.03.044. PubMed
1016 PMID: 30970250; PubMed Central PMCID: PMCPMC6459000.
1017 70. Peters MJ, Joehanes R, Pilling LC, Schurmann C, Conneely KN, Powell J, et al. The
1018 transcriptional landscape of age in human peripheral blood. Nature communications.
1019 2015;6:8570. Epub 2015/10/23. doi: 10.1038/ncomms9570. PubMed PMID: 26490707; PubMed
1020 Central PMCID: PMCPMC4639797.
1021 71. Svane AM, Soerensen M, Lund J, Tan Q, Jylhava J, Wang Y, et al. DNA Methylation and
1022 All-Cause Mortality in Middle-Aged and Elderly Danish Twins. Genes (Basel). 2018;9(2). Epub
1023 2018/02/09. doi: 10.3390/genes9020078. PubMed PMID: 29419728; PubMed Central PMCID:
1024 PMCPMC5852574.
1025 72. Zhang Y, Wilson R, Heiss J, Breitling LP, Saum KU, Schottker B, et al. DNA methylation
1026 signatures in peripheral blood strongly predict all-cause mortality. Nature communications.
1027 2017;8:14617. Epub 2017/03/18. doi: 10.1038/ncomms14617. PubMed PMID: 28303888;
1028 PubMed Central PMCID: PMCPMC5357865.
1029 73. Lund JB, Li S, Baumbach J, Svane AM, Hjelmborg J, Christiansen L, et al. DNA methylome
1030 profiling of all-cause mortality in comparison with age-associated methylation patterns. Clinical
1031 epigenetics. 2019;11(1):23. Epub 2019/02/10. doi: 10.1186/s13148-019-0622-4. PubMed PMID:
1032 30736859; PubMed Central PMCID: PMCPMC6368749.
1033 74. Bojesen SE, Timpson N, Relton C, Davey Smith G, Nordestgaard BG. AHRR (cg05575921)
1034 hypomethylation marks smoking behaviour, morbidity and mortality. Thorax. 2017;72(7):646-
1035 53. Epub 2017/01/20. doi: 10.1136/thoraxjnl-2016-208789. PubMed PMID: 28100713; PubMed
1036 Central PMCID: PMCPMC5520281.
1037 75. McCartney DL, Hillary RF, Stevenson AJ, Ritchie SJ, Walker RM, Zhang Q, et al. Epigenetic
1038 prediction of complex traits and death. Genome biology. 2018;19(1):136. Epub 2018/09/28.
1039 doi: 10.1186/s13059-018-1514-1. PubMed PMID: 30257690; PubMed Central PMCID:
1040 PMCPMC6158884.
1041 76. Albanes D, Winick M. Are cell number and cell proliferation risk factors for cancer? J Natl
1042 Cancer Inst. 1988;80(10):772-4. Epub 1988/07/20. doi: 10.1093/jnci/80.10.772. PubMed PMID:
1043 3385783.
1044 77. Bartke A. Healthy aging: is smaller better? - a mini-review. Gerontology. 2012;58(4):337-
1045 43. Epub 2012/01/21. doi: 10.1159/000335166. PubMed PMID: 22261798; PubMed Central
1046 PMCID: PMCPMC3893695.
1047 78. Global BMIMC, Di Angelantonio E, Bhupathiraju Sh N, Wormser D, Gao P, Kaptoge S, et
1048 al. Body-mass index and all-cause mortality: individual-participant-data meta-analysis of 239
1049 prospective studies in four continents. Lancet. 2016;388(10046):776-86. Epub 2016/07/18. doi:

1050 10.1016/S0140-6736(16)30175-1. PubMed PMID: 27423262; PubMed Central PMCID:
1051 PMCPMC4995441.
1052 79. Lemez S, Wattie N, Baker J. Do "big guys" really die younger? An examination of height
1053 and lifespan in former professional basketball players. PloS one. 2017;12(10). doi: ARTN
1054 e0185617
1055 10.1371/journal.pone.0185617. PubMed PMID: WOS:000412029600029.
1056 80. McCay CM, Crowell MF, Maynard LA. The effect of retarded growth upon the length of
1057 life span and upon the ultimate body size. 1935. Nutrition. 1989;5(3):155-71; discussion 72.
1058 Epub 1989/05/01. PubMed PMID: 2520283.
1059 81. Nunney L. Size matters: height, cell number and a person's risk of cancer. P Roy Soc B-
1060 Biol Sci. 2018;285(1889). doi: ARTN 20181743
1061 10.1098/rspb.2018.1743. PubMed PMID: WOS:000448380800012.
1062 82. Wahl S, Drong A, Lehne B, Loh M, Scott WR, Kunze S, et al. Epigenome-wide association
1063 study of body mass index, and the adverse outcomes of adiposity. Nature. 2017;541(7635):81-
1064 6. Epub 2016/12/22. doi: 10.1038/nature20784. PubMed PMID: 28002404; PubMed Central
1065 PMCID: PMCPMC5570525.
1066 83. Barfield RT, Almli LM, Kilaru V, Smith AK, Mercer KB, Duncan R, et al. Accounting for
1067 population stratification in DNA methylation studies. Genet Epidemiol. 2014;38(3):231-41. Epub
1068 2014/01/31. doi: 10.1002/gepi.21789. PubMed PMID: 24478250; PubMed Central PMCID:
1069 PMCPMC4090102.
1070 84. Rakyan VK, Down TA, Balding DJ, Beck S. Epigenome-wide association studies for
1071 common human diseases. Nature reviews Genetics. 2011;12(8):529-41. Epub 2011/07/13. doi:
1072 10.1038/nrg3000. PubMed PMID: 21747404; PubMed Central PMCID: PMCPMC3508712.
1073 85. Lappalainen T, Greally JM. Associating cellular epigenetic models with human
1074 phenotypes. Nature reviews Genetics. 2017;18(7):441-51. Epub 2017/05/31. doi:
1075 10.1038/nrg.2017.32. PubMed PMID: 28555657.
1076 86. FastQC. Available from: https://www.bioinformatics.babraham.ac.uk/projects/fastqc/.
1077 87. Langmead B, Trapnell C, Pop M, Salzberg SL. Ultrafast and memory-efficient alignment
1078 of short DNA sequences to the human genome. Genome biology. 2009;10(3):R25. doi:
1079 10.1186/gb-2009-10-3-r25. PubMed PMID: 19261174; PubMed Central PMCID: PMC2690996.
1080 88. Li H, Handsaker B, Wysoker A, Fennell T, Ruan J, Homer N, et al. The Sequence
1081 Alignment/Map format and SAMtools. Bioinformatics. 2009;25(16):2078-9. doi:
1082 10.1093/bioinformatics/btp352. PubMed PMID: 19505943; PubMed Central PMCID:
1083 PMC2723002.
1084 89. Lassmann T, Hayashizaki Y, Daub CO. SAMStat: monitoring biases in next generation
1085 sequencing data. Bioinformatics. 2011;27(1):130-1. Epub 2010/11/20. doi:
1086 10.1093/bioinformatics/btq614. PubMed PMID: 21088025; PubMed Central PMCID:
1087 PMCPMC3008642.
1088 90. Lienhard M, Grimm C, Morkel M, Herwig R, Chavez L. MEDIPS: genome-wide differential
1089 coverage analysis of sequencing data derived from DNA enrichment experiments.
1090 Bioinformatics. 2014;30(2):284-6. doi: 10.1093/bioinformatics/btt650. PubMed PMID:
1091 24227674; PubMed Central PMCID: PMC3892689.
1092 91. Robinson MD, McCarthy DJ, Smyth GK. edgeR: a Bioconductor package for differential
1093 expression analysis of digital gene expression data. Bioinformatics. 2010;26(1):139-40. doi:

1094 10.1093/bioinformatics/btp616. PubMed PMID: 19910308; PubMed Central PMCID:
1095 PMC2796818.
1096 92. Ashbrook DG, Arends D, Mulligan MK, Williams EG, Lutz C, Valenzuela A, et al.
1097 Sequencing the BXD family, a cohort for experimental systems genetics and precision medicine.
1098 IBANGS MEETING: THE 20TH ANNUAL GENES, BRAIN & BEHAVIOR MEETING Rochester, MN,
1099 USA. 2018.
1100 93. Ashbrook DG, Arends D, Prins P, Mulligan MK, Roy S, Williams EG, et al. The expanded
1101 BXD family of mice: A cohort for experimental systems genetics and precision medicine.
1102 bioRxiv. 2019:672097. doi: 10.1101/672097.
1103 94. Heinz S, Benner C, Spann N, Bertolino E, Lin YC, Laslo P, et al. Simple combinations of
1104 lineage-determining transcription factors prime cis-regulatory elements required for
1105 macrophage and B cell identities. Molecular cell. 2010;38(4):576-89. Epub 2010/06/02. doi:
1106 10.1016/j.molcel.2010.05.004. PubMed PMID: 20513432; PubMed Central PMCID:
1107 PMCPMC2898526.
1108 95. Liao Y, Wang J, Jaehnig EJ, Shi Z, Zhang B. WebGestalt 2019: gene set analysis toolkit
1109 with revamped UIs and APIs. Nucleic acids research. 2019;47(W1):W199-W205. Epub
1110 2019/05/23. doi: 10.1093/nar/gkz401. PubMed PMID: 31114916; PubMed Central PMCID:
1111 PMCPMC6602449.
1112 96. Zhang B, Kirov S, Snoddy J. WebGestalt: an integrated system for exploring gene sets in
1113 various biological contexts. Nucleic acids research. 2005;33(Web Server issue):W741-8. Epub
1114 2005/06/28. doi: 10.1093/nar/gki475. PubMed PMID: 15980575; PubMed Central PMCID:
1115 PMCPMC1160236.
1116 97. Bates D, Maechler M, Bolker B, Walker S. lme4: Linear mixed-effects models using Eigen
1117 and S4. . R package version 11-7, http://CRANR-projectorg/package=lme4.
1118 98. Friedman J, Hastie T, Tibshirani R. Regularization Paths for Generalized Linear Models via
1119 Coordinate Descent. J Stat Softw. 2010;33(1):1-22. Epub 2010/09/03. PubMed PMID:
1120 20808728; PubMed Central PMCID: PMCPMC2929880.
1121 99. Zou H, Hastie T. Regularization and variable selection via the elastic net. Journal of the
1122 Royal Statistical Society: Series B (Statistical Methodology). 2005;67(2):301-20. doi:
1123 10.1111/j.1467-9868.2005.00503.x.
1124 100. NIA Aging BXD CD+HFD Liver RNA-Seq (Aug18) Log2.
1125

1126

1127

1128

1129

1130

1131

1132 # Figure legends.

1133 **Fig. 1. Age distribution and body weight characteristics.**

1134 **(a)** Each point depicts a mouse used for methylome assay. The purpose of this plot is to show a

1135 near uniform distribution of ages (y-axis) across the three lifespan groups (categorical

1136 classification on x-axis; short-lived with strain mean lifespan < 600 days, medium-lived: 640–

1137 750 days, and long-lived: lifespan > 800 days).

1138 **(b)** The bar plots show significant strain variation in mean body weight at young adulthood

1139 (baseline weight) and at final weighing. By final weight, mice on high fat diet (HFD) had gained

1140 significant weight. The weight of the liver did not differ significantly between strains and

1141 showed only a slight gain for mice on HFD. These graphs were plotted using all 70 samples;

1142 excluding the three male cases in BXD102, B6D2F1, and D2B6F1, did not alter the strain

1143 distribution and the F1s still had robust body weights.

1144 **(c)** At young adulthood, body weight was significantly correlated with age of mice. The baseline

1145 body weight was also correlated with final weight of body **(d)** and liver **(e)**.

1146

1147 **Fig. 2. Global features of the methylome**

1148 **(a)** Scatter plot between the top 2 principal components—PC1 (19% of variance) and PC2 (13%

1149 of variance)—show a strong population structure with mice clustering by strain identity (color

1150 coded). Members of sub-strains also cluster in close proximity. For strains with animals from

1151 both standard chow (CD; solid circles) and high fat diet (HFD; squares), mice on HFD co-cluster

1152 with the CD mice.

1153 For each individual mouse, the overall mean methylation and within-individual variance was
1154 calculated for 200,531 genic CpG regions located with annotated genes **(b)**, and 167,769 CpG
1155 regions in intergenic sites **(c)**. The intergenic regions have wide variation between strains and
1156 the F1 hybrids have the highest mean methylation and lowest variance. The genic CpG regions
1157 are more consistent across strains. Scatter plots on the right show the correlation between
1158 methylation averages and variance in the 70 samples. Mean methylation is inversely correlated
1159 with variance, and this is particularly pronounced for the intergenic CpG regions. Average
1160 methylation at intergenic regions (x-axis) is correlated with PC1 **(d)**, and PC3 **(e)**, and average
1161 methylation at genic regions is correlated with PC4 **(f)**.
1162
1163 **Fig. 3. Intercorrelation between body weight at young adulthood, the methylome, and strain**
1164 **longevity**
1165 Body weight at young adulthood has weak but significant correlations with **(a)** the methylome
1166 top principal component, PC1, and the **(b)** mean methylation and **(c)** variance at genic CpG
1167 regions. Given the timeline, the results indicate that the body weight at earlier time is
1168 predictive of DNA methylation (solid arrow). However, since both are genetically modulated
1169 phenotypes and the methylome may also have had a sustained effect on the body weight of
1170 mice (dashed arrow), the direction of causality cannot be clearly resolved, and we consider
1171 these as interdependent phenotypes.
1172 **(d)** The methylome in turn may be predictive of lifespan (solid arrow), and PC4, a correlate of
1173 mean methylation at genic CpG regions, is strongly correlated with lifespan.

1174 **(e)** Baseline body weight is also predictive of strain longevity (solid arrow), and the negative
1175 correlation conveys reduced lifespan for mice that had heavier body weight at young
1176 adulthood.
1177
1178 **Fig. 4. Features of age dependent differentially methylated CpGs regions (age-DMRs)**
1179 **(a)** Histogram of observed *p*-values for age dependent methylation shows that aging has a
1180 strong effect on few CpG regions. **(b)** The *p*-values for the effect of diet showed a null
1181 distribution, likely because of the small number of samples from mice kept on high fat diet
1182 **(c)** Each point in the Manhattan plot depicts the location of a CpG region (x-axis: autosomal
1183 chromosomes 1 to 19; and chromosome X as 20), and the $-\log_{10}p$ for age effect (y-axis). The
1184 genome-wide significant threshold was set at $-\log_{10}(2.6e\text{-}7)$ (red line; 10% Bonferroni threshold
1185 for 368,300 tests) and the suggestive threshold at $-\log_{10}(3.6e\text{-}4)$ (blue line). **(d)** The top 500 age-
1186 DMRs consisted of 206 regions that gained methylation with age (age-hypermethylated;
1187 positive regression coefficient for age), and 294 regions that were age-hypomethylated
1188 (negative regression coefficient for age). The bar-plots display the percent total of genomic
1189 features in the age-hypermethylated (burgundy) and age-hypomethylated (sandy brown) sets,
1190 relative to the set of 369,300 MBD-seq bins (grey), and the full genome-wide background set
1191 (black). Within the bins, the regression coefficients for age (i.e., change in DNA methylation per
1192 unit change in age in days, $\log_{10}$ scale) were dependent on the **(e)** CpG density, and **(f)** mean
1193 methylation.
1194
1195 **Fig. 5. Elastic net regression DNA methylation and mRNA clocks**

1196 The y-axis shows the chronological age of mice, and the x-axis shows the DNAmAges predicted
1197 by the 60 clock CpG regions in the **(a)** training set of 36 samples, and **(b)** the testing set of 33
1198 samples.
1199 For the transcriptomic data, the training in 150 RNA-seq samples (batch 1) identified 65
1200 transcripts for age estimation. The plots compare the chronological ages to the predicted ages
1201 in the **(c)** training set of 150 samples, and **(d)** in the testing testing of 140 samples (batch 2). To
1202 complement this, the training was also carried out in the 140 samples (batch 2) and this
1203 identified 62 transcripts for age estimation. Correlations between chronological age and
1204 estimated age in the batch 2 training set (**e**), and batch 1 testing set (**f**) are shown.
1205
1206 **Fig. 6. DNA methylation based epigenetic clocks derived from age-DMRs**
1207 The epigenetic age of mice was estimated from DNA methylation levels at the 500 age-DMRs.
1208 **(a)** The estimated DNAmAge (y-axis) was correlated with chronological age (x-axis) of mice. The
1209 age acceleration residuals (DNAmAge-acc) derived from this clock **(b)** did not correlate with
1210 strain lifespan, **(c)** but was positively correlated with body weight. **(d)** For strains with samples
1211 from both standard chow (control diet or CD) and high fat diet (HFD), the DNAmAge-acc did not
1212 differentiate between the diet groups.
1213 A second version of the clock was made using 56 age-DMRs that were also associated with
1214 lifespan variation. **(e)** The DNAmAge derived for the 56 age-lifespan-DMRs correlated with
1215 chronological age on mice; however, the relation deviated from linearity and appeared to
1216 plateau for the older mice. The DNAmAge-acc from this clock was **(f)** inversely correlated with
1217 strain lifespan that indicates decelerated aging in long-lived strains, and **(g)** positively correlated

1218 with baseline body weight that suggests a more accelerated clock for mice with higher body
1219 weight at younger age. **(h)** This clock also indicates greater age acceleration for the HFD group
1220 compared to the CD group (mean of 21 ± 36 for HFD, -26 ± 57 for CD; p = 0.01; n = 33).
1221
1222 **Fig. 7. Lifespan predictive age-DMRs**
1223 **(a)** Comparison between the regression coefficients for age (x-axis) vs. the regression
1224 coefficient for strain median lifespan (y-axis) shows that most of the age-DMRs that are also
1225 associated with lifespan have generally lower methylation levels in strains with longer median
1226 lifespan, as indicated by the negative regression coefficient for lifespan. As examples of age and
1227 lifespan associated CpG regions, the change in methylation over time along with cross-sectional
1228 variation is illustrated by the age-hypomethylated CpG region in **(b)** *Casz1*, and by the age-
1229 hypermethylated CpG regions in **(c)** *Cyp46a1* and **(d)** *Abca7*. Each point represents a mouse
1230 plotted by age (x-axis) and methylation level (y-axis, logRPKM). The lines represent linear
1231 regression lines for each strain-by-diet, classified by strain lifespan phenotype as short- (red),
1232 medium (yellow) or long-lived (blue). In all three CpG regions, cross-sectional comparisons
1233 show that mice belonging to short-lived groups have higher average methylation relative to
1234 mice belong to medium and long-lived groups (box plots). *Casz1* mean methylation log RPKM in
1235 short-lived = 3.96 ± 0.28, medium-lived = 3.62 ± 0.39, long-lived = 3.28 ± 0.42 (ANOVA p <
1236 0.0001. *Cyp46a1* mean methylation log RPKM in short-lived = 3.34 ± 0.69, medium-lived = 3.08
1237 ± 0.85, long-lived = 2.51 ± 0.83 (p = 0.0025. *Abca7* mean methylation log RPKM in short-lived =
1238 3.85 ± 0.41, medium-lived = 3.75 ± 0.33, long-lived = 3.58 ± 0.32 (p = 0.04).
1239

1240 **Fig. 8. Epigenetic clock derived from body weight associated CpG regions**

1241 **(a)** The Manhattan plot for baseline body weight (BW0) shows widespread association with

1242 DNA methylation. The genome-wide significant threshold is set at $-\log_{10}(2.6e-7)$ (red line; 10%

1243 Bonferroni threshold for 368,300 tests).

1244 The epigenetic clock was estimated from DNA methylation levels at the top 500 BW0 associated

1245 CpG regions. **(b)** We refer to this version of the clock as BW0.lifespan as the estimates (y-axis)

1246 has a significant positive correlation with the expected lifespan of strains (x-axis). However, for

1247 the long-lived F1 hybrids and BXD65 cases that also had higher body weight, the estimates were

1248 shorter than the recorded lifespans (cluster A has B6D2F1 and BXD65, cluster B has D2B6F1). **(c)**

1249 Baseline body weight (x-axis) is negatively correlated with the BW0.lifespan estimates. **(d)** Age-

1250 acceleration from the 56 lifespan-age-DMR clock (x-axis) was negatively correlated with the

1251 BW0.lifespan estimated with more accelerated epigenetic aging for shorter-lived BXDs.

1252

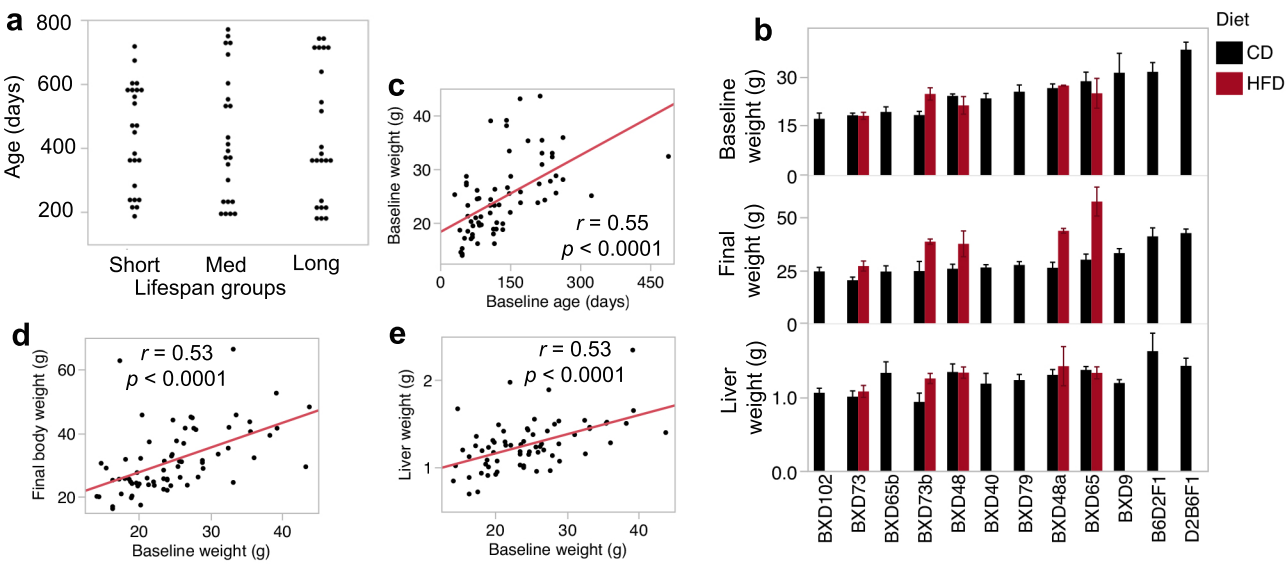
a
Age (days)
800
600
400
200
Short
Med
Long
Lifespan groups
b
Diet
CD
HFD
Baseline weight (g)
Final weight (g)
Liver weight (g)
BXD102
BXD73
BXD65b
BXD73b
BXD48
BXD40
BXD79
BXD48a
BXD65
BXD9
B6D2F1
D2B6F1
c
Baseline weight (g)
Baseline age (days)
r = 0.55
p < 0.0001
d
Final body weight (g)
Baseline weight (g)
r = 0.53
p < 0.0001
e
Liver weight (g)
Baseline weight (g)
r = 0.53
p < 0.0001

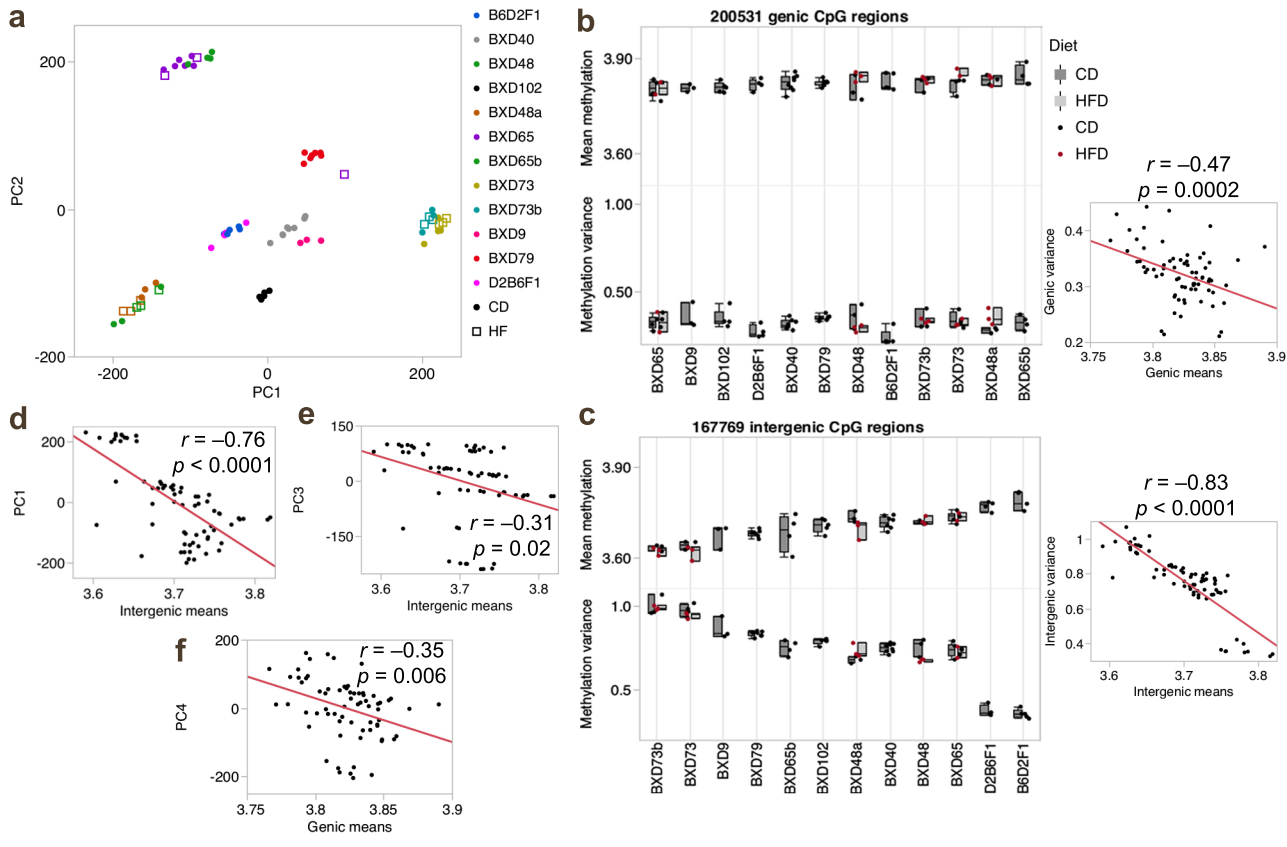
a
B6D2F1
BXD40
BXD48
BXD102
BXD48a
BXD65
BXD65b
BXD73
BXD73b
BXD9
BXD79
D2B6F1
CD
HF
PC1
PC2
b
200531 genic CpG regions
Mean methylation
Methylation variance
Diet
CD
HFD
CD
HFD
BXD65
BXD9
BXD102
D2B6F1
BXD40
BXD79
BXD48
B6D2F1
BXD73b
BXD73
BXD48a
BXD65b
r = –0.47
p = 0.0002
Genic variance
Genic means
c
167769 intergenic CpG regions
Mean methylation
Methylation variance
BXD73b
BXD73
BXD9
BXD79
BXD65b
BXD102
BXD48a
BXD40
BXD48
BXD65
D2B6F1
B6D2F1
r = –0.83
p < 0.0001
Intergenic variance
Intergenic means
d
r = –0.76
p < 0.0001
PC1
Intergenic means
e
r = –0.31
p = 0.02
PC3
Intergenic means
f
r = –0.35
p = 0.006
PC4
Genic means

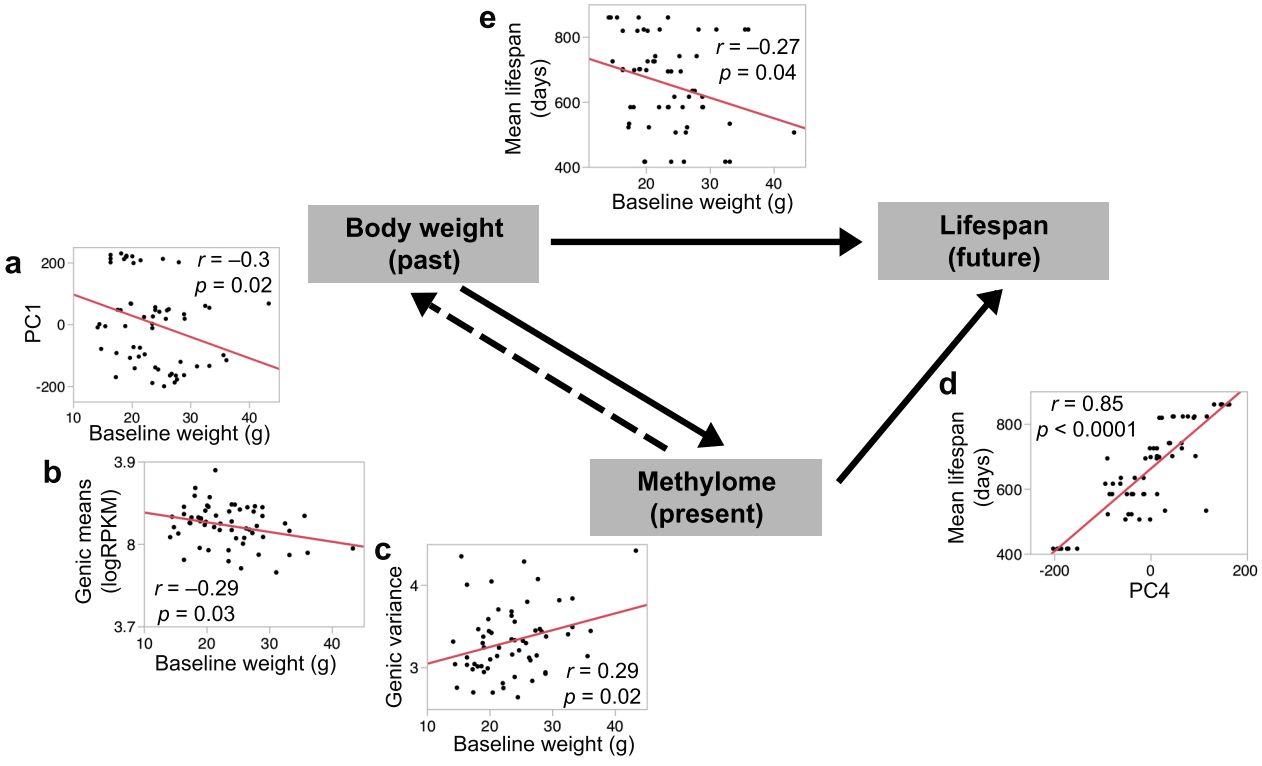
e
Mean lifespan (days)
800
600
400
r = –0.27
p = 0.04
20
30
40
Baseline weight (g)
Body weight (past)
Lifespan (future)
a
PC1
200
0
-200
r = –0.3
p = 0.02
10
20
30
40
Baseline weight (g)
b
Genic means (logRPKM)
3.9
8
3.7
r = –0.29
p = 0.03
10
20
30
40
Baseline weight (g)
Methylome (present)
c
Genic variance
4
3
r = 0.29
p = 0.02
10
20
30
40
Baseline weight (g)
d
Mean lifespan (days)
800
600
400
r = 0.85
p < 0.0001
-200
0
200
PC4

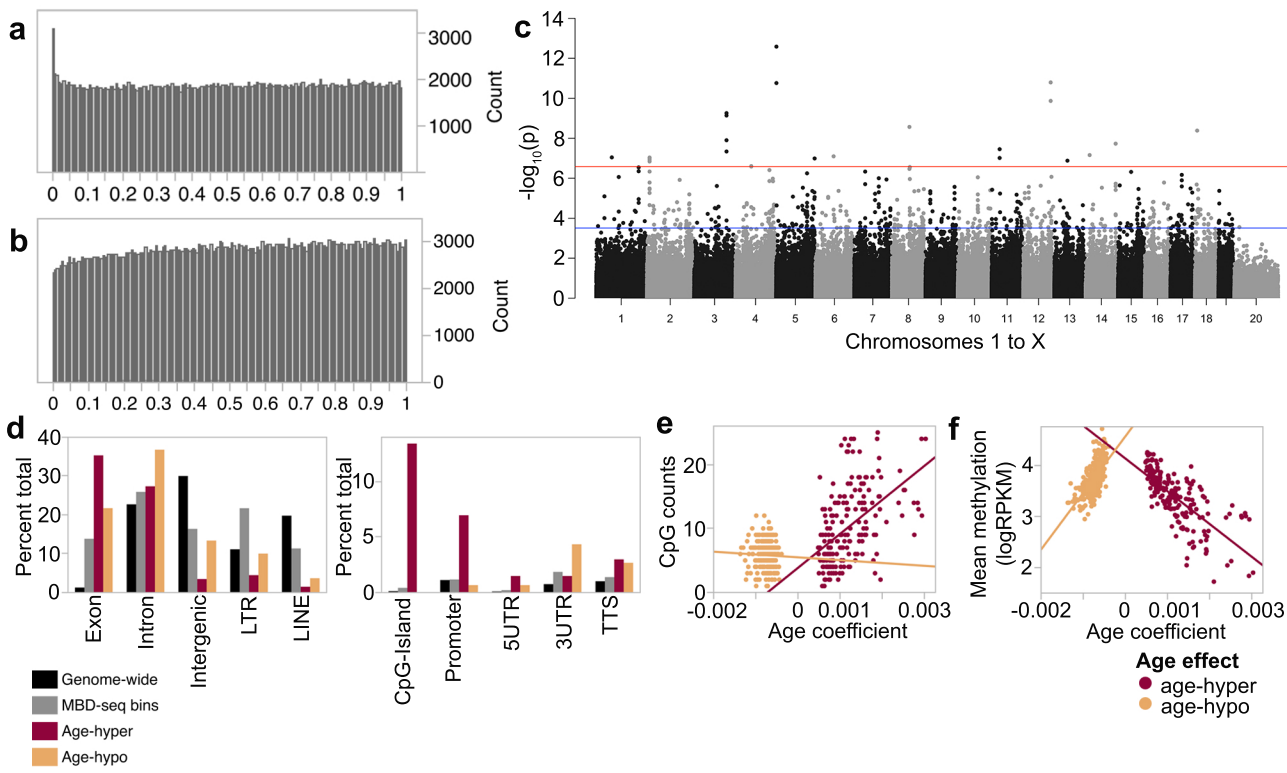
a
Count
3000
2000
1000
0 0.1 0.2 0.3 0.4 0.5 0.6 0.7 0.8 0.9 1
b
Count
3000
2000
1000
0
0 0.1 0.2 0.3 0.4 0.5 0.6 0.7 0.8 0.9 1
c
-log10(p)
14
12
10
8
6
4
2
0
1 2 3 4 5 6 7 8 9 10 11 12 13 14 15 16 17 18 20
Chromosomes 1 to X
d
Percent total
40
30
20
10
0
Exon
Intron
Intergenic
LTR
LINE
Percent total
10
5
0
CpG-Island
Promoter
5UTR
3UTR
TTS
Genome-wide
MBD-seq bins
Age-hyper
Age-hypo
e
CpG counts
20
10
0
-0.002 0 0.001 0.003
Age coefficient
f
Mean methylation (logRPKM)
4
3
2
-0.002 0 0.001 0.003
Age coefficient
Age effect
age-hyper
age-hypo

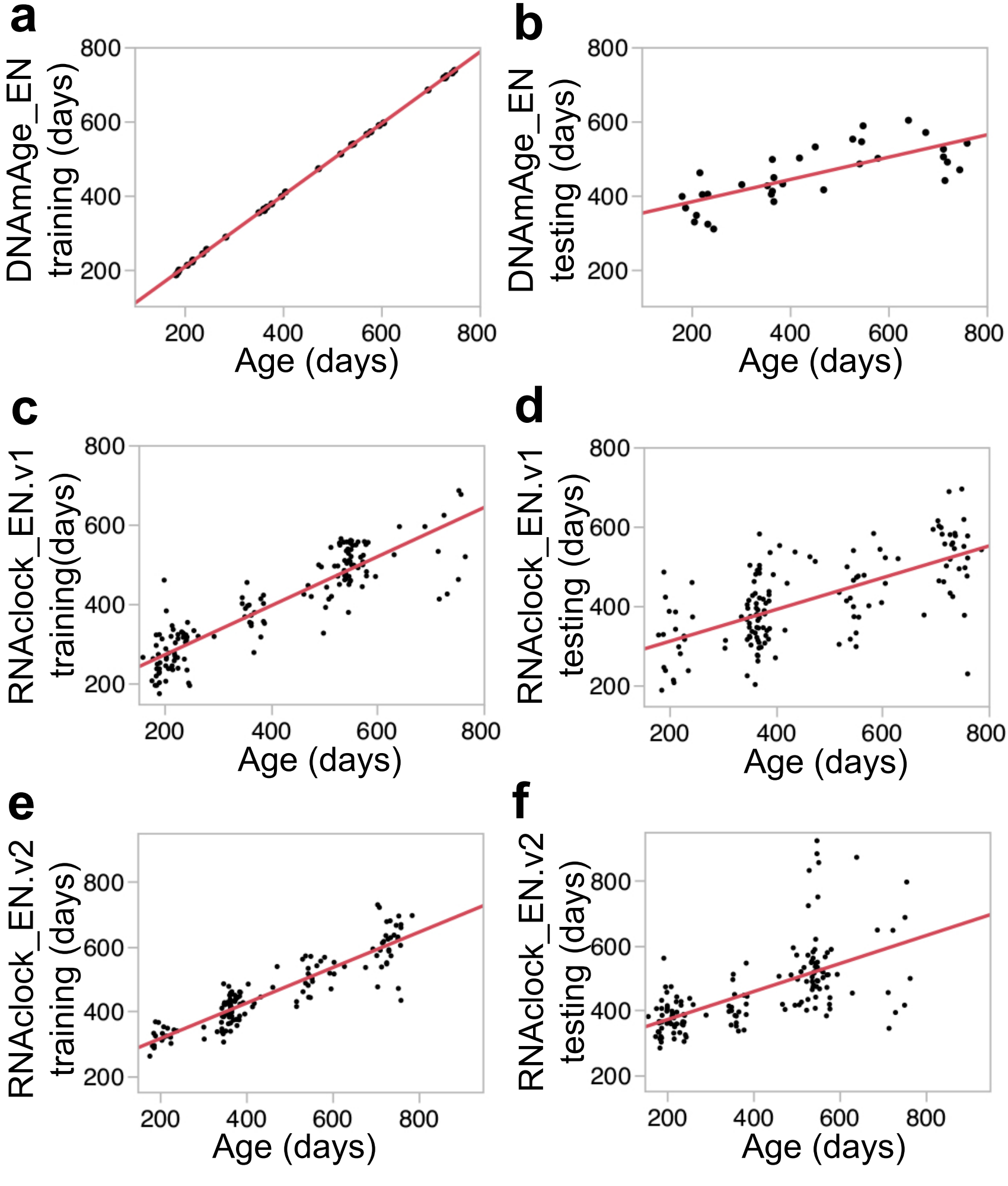
a
DNAmAge_EN
training (days)
800
600
400
200
200
400
600
800
Age (days)
b
DNAmAge_EN
testing (days)
800
600
400
200
200
400
600
800
Age (days)
c
RNAclock_EN.v1
training(days)
800
600
400
200
200
400
600
800
Age (days)
d
RNAclock_EN.v1
testing (days)
800
600
400
200
200
400
600
800
Age (days)
e
RNAclock_EN.v2
training (days)
800
600
400
200
200
400
600
800
Age (days)
f
RNAclock_EN.v2
testing (days)
800
600
400
200
200
400
600
800
Age (days)

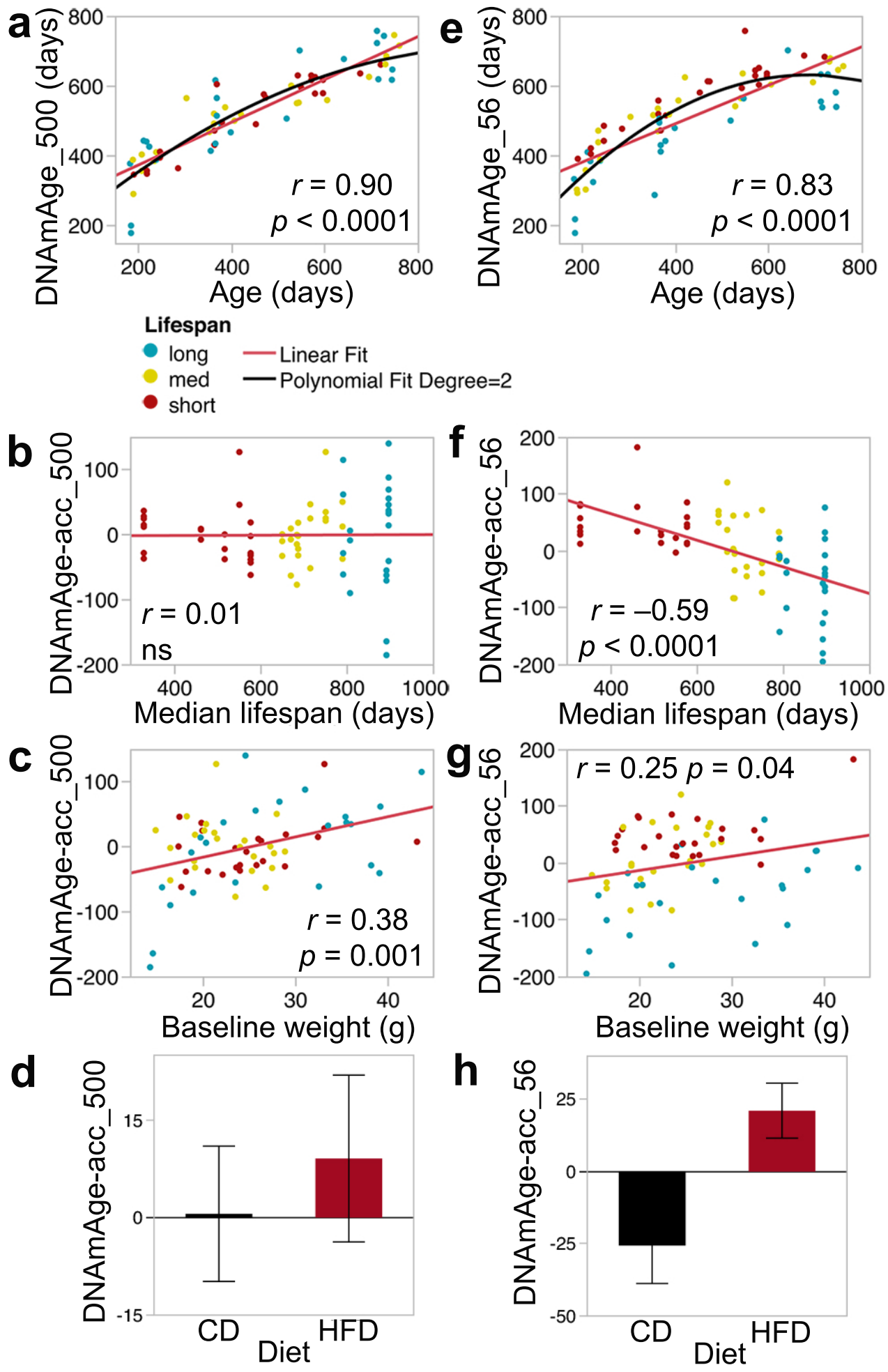
a
DNAmAge_500 (days)
Age (days)
r = 0.90
p < 0.0001
e
DNAmAge_56 (days)
Age (days)
r = 0.83
p < 0.0001
Lifespan
long
med
short
Linear Fit
Polynomial Fit Degree=2
b
DNAmAge-acc_500
Median lifespan (days)
r = 0.01
ns
f
DNAmAge-acc_56
Median lifespan (days)
r = –0.59
p < 0.0001
c
DNAmAge-acc_500
Baseline weight (g)
r = 0.38
p = 0.001
g
DNAmAge-acc_56
Baseline weight (g)
r = 0.25 p = 0.04
d
DNAmAge-acc_500
CD
HFD
Diet
h
DNAmAge-acc_56
CD
HFD
Diet

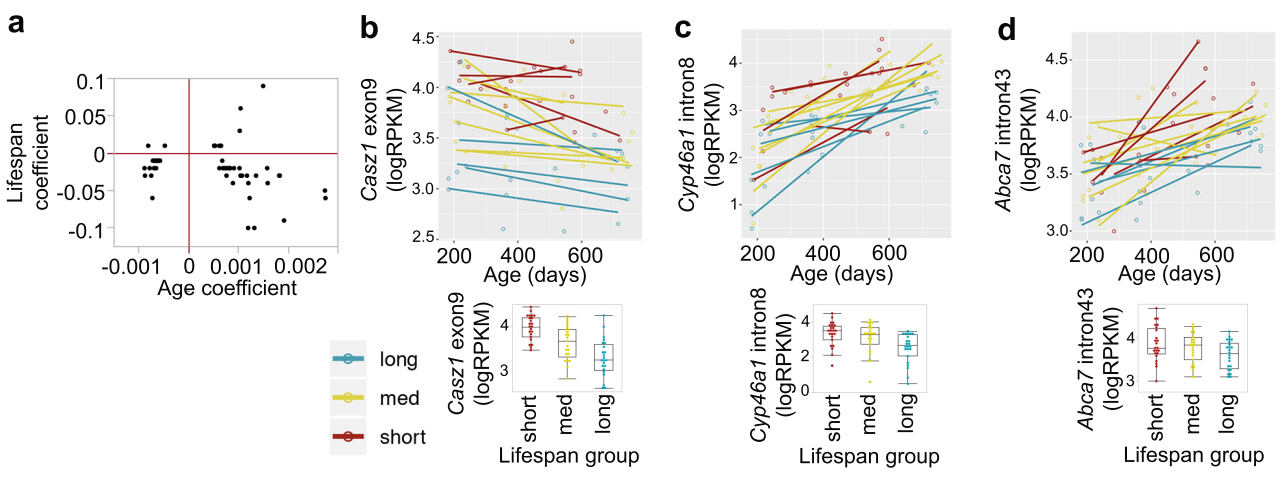
a
Lifespan coefficient
0.1
0.05
0
-0.05
-0.1
-0.001
0
0.001
0.002
Age coefficient
b
Casz1 exon9 (logRPKM)
4.5
4.0
3.5
3.0
2.5
200
400
600
Age (days)
Casz1 exon9 (logRPKM)
4
3
short
med
long
Lifespan group
c
Cyp46a1 intron8 (logRPKM)
4
3
2
1
200
400
600
Age (days)
Cyp46a1 intron8 (logRPKM)
4
2
0
short
med
long
Lifespan group
d
Abca7 intron43 (logRPKM)
4.5
4.0
3.5
3.0
200
400
600
Age (days)
Abca7 intron43 (logRPKM)
4
3
short
med
long
Lifespan group
long
med
short

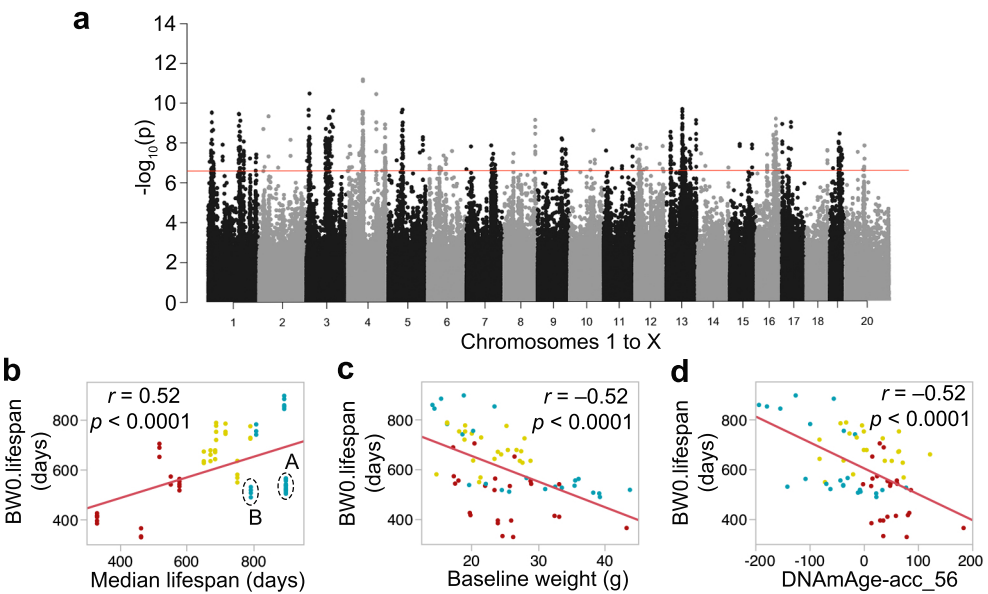
a
-log10(p)
Chromosomes 1 to X
b
r = 0.52
p < 0.0001
BW0.lifespan (days)
Median lifespan (days)
A
B
c
r = –0.52
p < 0.0001
BW0.lifespan (days)
Baseline weight (g)
d
r = –0.52
p < 0.0001
BW0.lifespan (days)
DNAmAge-acc_56

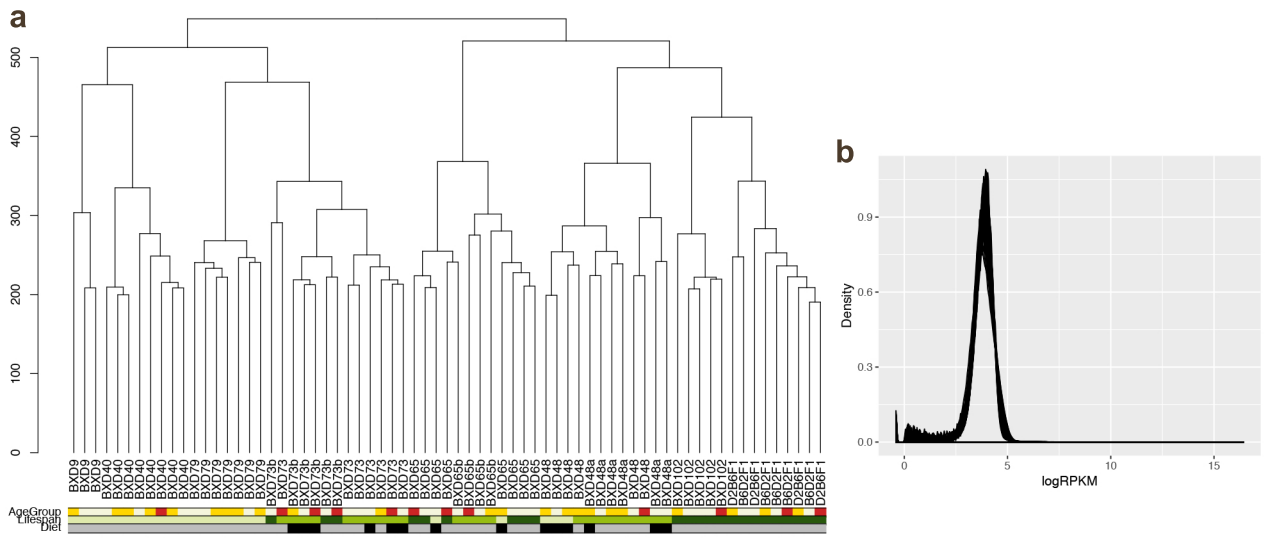
a
500
400
300
200
100
0
AgeGroup
Lifespan
Diet
b
Density
0.9
0.6
0.3
0.0
0
5
10
15
logRPKM

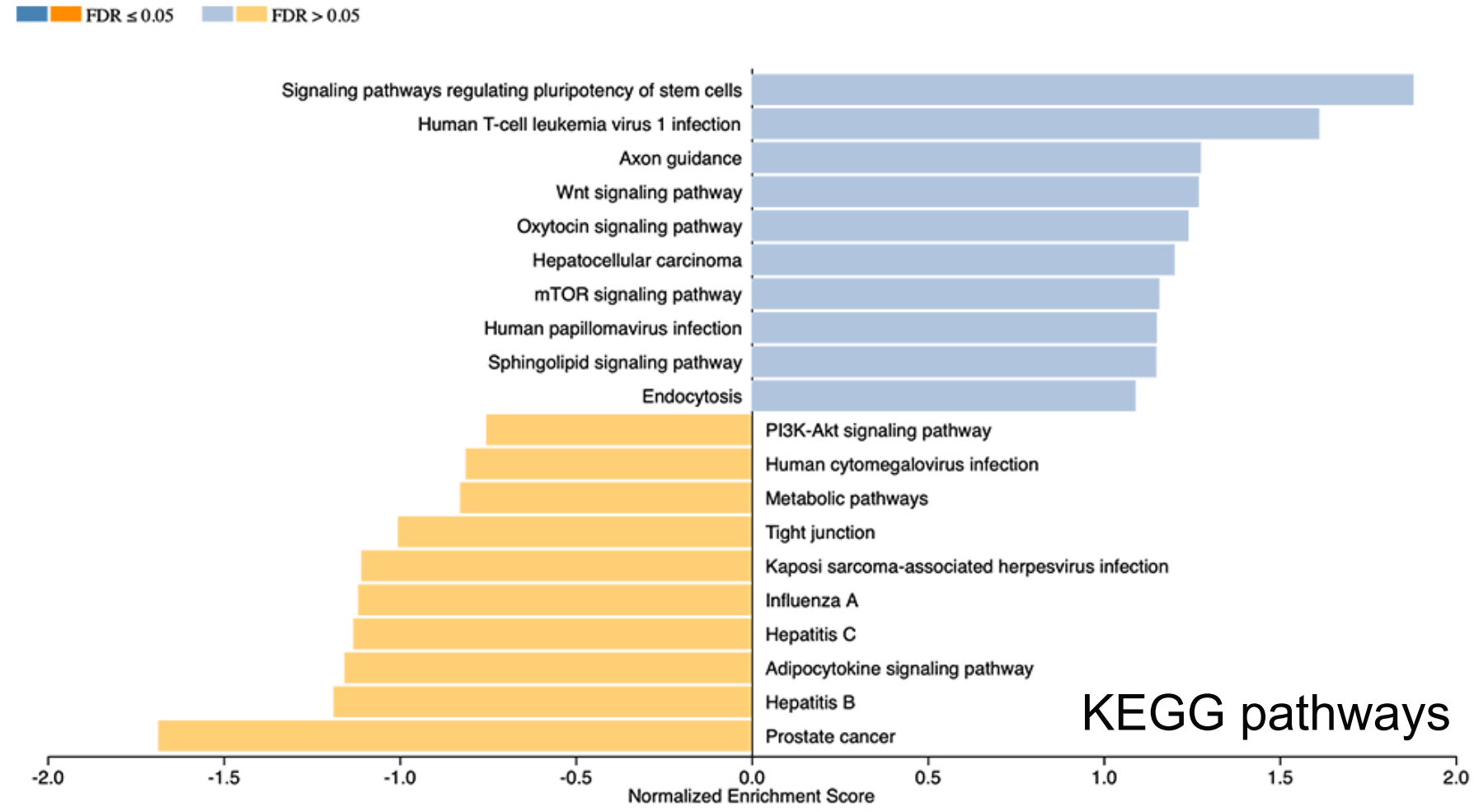
FDR ≤ 0.05
FDR > 0.05
Signaling pathways regulating pluripotency of stem cells
Human T-cell leukemia virus 1 infection
Axon guidance
Wnt signaling pathway
Oxytocin signaling pathway
Hepatocellular carcinoma
mTOR signaling pathway
Human papillomavirus infection
Sphingolipid signaling pathway
Endocytosis
PI3K-Akt signaling pathway
Human cytomegalovirus infection
Metabolic pathways
Tight junction
Kaposi sarcoma-associated herpesvirus infection
Influenza A
Hepatitis C
Adipocytokine signaling pathway
Hepatitis B
Prostate cancer
KEGG pathways
-2.0
-1.5
-1.0
-0.5
0.0
0.5
1.0
1.5
2.0
Normalized Enrichment Score

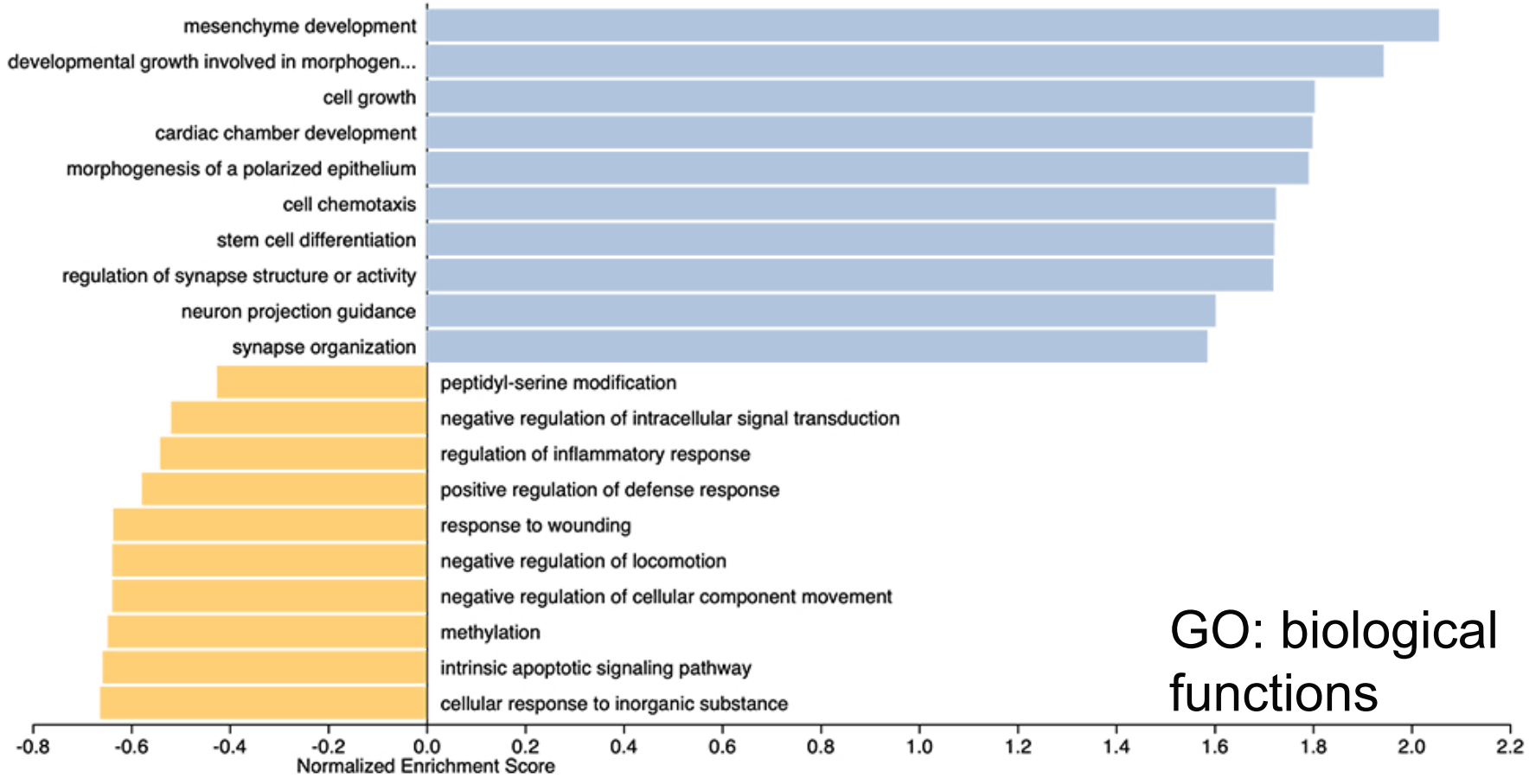
mesenchyme development
developmental growth involved in morphogen...
cell growth
cardiac chamber development
morphogenesis of a polarized epithelium
cell chemotaxis
stem cell differentiation
regulation of synapse structure or activity
neuron projection guidance
synapse organization
peptidyl-serine modification
negative regulation of intracellular signal transduction
regulation of inflammatory response
positive regulation of defense response
response to wounding
negative regulation of locomotion
negative regulation of cellular component movement
methylation
intrinsic apoptotic signaling pathway
cellular response to inorganic substance
GO: biological functions
-0.8
-0.6
-0.4
-0.2
0.0
0.2
0.4
0.6
0.8
1.0
1.2
1.4
1.6
1.8
2.0
2.2
Normalized Enrichment Score